Gold Nanoparticle Functionalized Surfaces for Plasmon-Enhanced Fluorescence Detection of Nucleic Acids

Tiago Miguel Soares Policarpo

Thesis to obtain the Master of Science Degree in

Biotechnology

Supervisors: Professor João Pedro Estrela Rodrigues Conde

Doctor Pedro Miguel Neves Ribeiro Paulo

Examination Committee:

Chairperson: Professor Marília Clemente Velez Mateus

Supervisor: Doctor Pedro Miguel Neves Ribeiro Paulo

Member of the Committee: Professor Duarte Miguel de França Teixeira dos Prazeres

November of 2018

Agradecimentos

Esta tese marca o fim de uma etapa muito importante da minha vida, por isso não podia deixar de agradecer a todos os que desempenharam um papel importante.

Antes demais gostaria de agradecer aos meus co-orientadores, o Professor João Pedro Conde e o Doutor Pedro Paulo, pela oportunidade que me foi dada de aprender sobre um tema que até há pouco tempo me era desconhecido. Um obrigado em especial ao Doutor Pedro Paulo por toda a paciência que demonstrou para comigo e por tudo o que me ensinou ao longo destes últimos meses. Agradeço muito também a ajuda do Mestre David Botequim e do Mestre Rui Silva, pela prontidão em me esclarecerem dúvidas, partilharem do seu conhecimento e me acompanharem em experiências quando precisei de ajuda. Os meus sinceros agradecimentos à Doutora Vanda Vaz Serra e à Doutora Sílvia Costa por toda a simpatia que demonstraram para comigo desde o início, que me fez sentir muito bem-vindo no grupo de investigação.

Um agradecimento especial a todos os meus colegas de curso, com quem partilhei esta experiência e que sempre me apoiaram ao longo destes anos e com quem criei fortes laços de amizade.

Um obrigado com muito carinho à Mariana Guttiérrez, por todo o apoio incondicional que me deu ao longo destes anos.

Um agradecimento do fundo do coração à minha avó Joaquina por ter partilhado esta experiência da universidade comigo e por ser uma grande companheira de casa.

E por último, mas de todo não menos importante gostava de agradecer à minha mãe por tudo o que fez por mim e me ter tornado no que sou hoje. És e para sempre serás a minha heroína.

Resumo

O uso de nanoestruturas metálicas como antenas ópticas para a intensificação de fluorescência, é um tópico de interesse para a comunidade científica. O fenómeno de fluorescência intensificada por metal promete melhorar as nossas capacidades de detecção de fluorescência atuais e permitir a criação de sensores mais sensíveis.

Dímeros de nanopartículas de ouro despertam especial interesse, visto que conseguem concentrar luz no seu interstício, criando campos elétricos muito fortes. O plasmão é capaz de promover grandes efeitos de intensificação de fluorescência. Sendo assim, filmes compactos de nanopartículas que podem induzir intensificações parecidas com as de dímeros em largas áreas, despertam interesse.

Aqui, dímeros foram formados, usando cadeias de DNA como espaçadores, com resultados moderados. Experiências de intensificação de fluorescência foram realizadas usando “nanorods” de ouro para amplificar a emissão de dois fluoróforos, a ftalocianina tetrasulfonada de alumínio e o ATTO-647N, obtendo factores de intensificação na ordem das 200 a 80 vezes respetivamente.

Filmes compactos foram preparados, usando um método de deposição baseado na auto-organização de nanopartículas e posteriormente testados para caracterizar a sua capacidade de intensificar a fluorescência, usando o “beacon” molecular BF1-BD2-TD e o espaçador de DNA BF1-BT, marcados com ATTO-647N. Os resultados obtidos, sugerem obtenção de alguma regularidade nas superfícies, com áreas densamente organizadas, tornando-as adequadas apara a intensificação de fluorescência.

Embora melhorias na organização de nanopartículas e na área coberta ainda sejam necessárias, os filmes produzidos constituem um passo promissor para a criação de substratos que possam ser usados para aumentar a sensibilidade de sensores de fluorescência.

Palavras-chaves: Fluorescência intensificada por metal; Nanopartículas de ouro; Filmes de nanopartículas;

Abstract

The use of metallic nanostructures as optical antennas to intensify the fluorescence of molecules, has been a topic of interest amongst the scientific community. The phenomenon of metal-enhanced fluorescence promises to greatly improve our current capabilities of fluorescence detection and therefore enable the creation of more sensitive sensors.

Dimers of gold nanoparticles are of special interest, as these structures can concentrate light to yield large electric fields in the gap between the two particles. The plasmon nearfield promotes large effects of fluorescence enhancement in dye molecules or other emitters. Therefore, closely packed films of nanoparticles which could induce nearfield enhancements similar to those produced by dimers, but over a larger area, are of great interest.

Nanoparticles dimers were prepared, using DNA strands as molecular linkers, with moderate results. Furthermore, experiments of fluorescence enhancement were performed using gold nanorods to amplify the emission from two fluorophores, aluminium tetrasulfonated phthalocyanine and ATTO-647N, obtaining maximum enhancement factors of around 200 and 80 times, respectively.

Closely packed gold nanoparticle films were then prepared using an air-liquid interface organization deposition method. These were tested to characterize their fluorescence enhancement abilities using the molecular beacon BF1-BD2-TD and the DNA spacer BF1-BT, labelled with ATTO-647N fluorophore. The results suggest the surface areas of highly-dense organized nanoparticles making them suitable for fluorescence enhancement. Although some improvements in particle organization and surface coverage are required, the films developed here constitute a promising step toward a plasmonic substrate that could be used for increasing sensitivity in fluorescence-based sensor devices.

Keywords: Metal-enhanced fluorescence; Gold nanoparticles; Nanoparticle films;

Table of Contents

Table of Tables

Table of Figures

Abbreviations

AlPcTS – Aluminium Tetrasulfonated Phthalocyanine;
AuNP – Gold Nanoparticle;
AuNR – Gold Nanorod;
AUT – 11-Amino-1-undecanethiol hydrochloride
BSPP - Bis(p-sulfonatophenyl)phenylphosphine dihydrate dipotassium salt
FCS – Fluorescence Correlation Spectroscopy;
FLIM – Fluorescence-lifetime Imaging Microscopy;
IRF – Instrument Response Function;
LSP – Localized Surface Plasmon;
LSPR – Localized Surface Plasmon Resonance;
MCS – Multi-Channel-Scalers*;*
MEF – Metal-Enhanced Fluorescence;
nt – nucleotides;
OD – optic density;
PBS – Phosphate buffered saline;
PEF – Plasmon-Enhanced Fluorescence;
rpm – rotations per minute;
SEM – Scanning Electron Microscopy
SPAD – Single Photon Avalanche Diode;
TBE – Tris-Borate-EDTA;
TCEP - Tris(2-carboxyethyl) phosphine hydrochloride
TCSPC – Time Correlated Single Photon Counting;
TEM – Transmission Electron Microscopy;

1. Introduction

A sensor can be defined as a system whose purpose is the detection of specific events from the surrounding environment in a broad sense and provide a signal of some sort. Many natural examples of this definition can be provided, for instance, our eyes can detect light derived from the environment external to us and then feed a signal to the brain for interpretation of the data received.

Mankind has since, taken this concept and applied it to situations deemed important. Furthermore, many types of sensors have been developed to detect different physical or chemical properties. For instance, there are sensors based on pressure difference, temperature, or based on the detection of target analytes, such as toxins, explosives, virus, bacteria, or other disease biomarkers [1].

The advances in molecular fluorescence allowed for the manufacturing of optical sensors that are able to probe events at the molecular level. With this type of technology, now widespread across almost all fields, enabling us to control environmental pollution, industrial product quality, and food contamination, among other. But one of the most significant impacts of this technology was in the biological and medical fields. Being able to detect small molecules meant that we could now detect biological molecules, much like what happens when using an enzyme-linked immunosorbent assay (ELISA) assay, which uses luminescence as an optical signal. So, many diseases or infections could now be detected using this technology.

In this sense, the discovery of disease biomarkers is fundamental for the development of biosensors that can be used as a diagnostic tool. Many disease biomarkers have been reported in the literature, including for one of the major causes of death worldwide nowadays, cancer. For instance, the finding of micro-RNAs circulating in the bloodstream of the patient that could be used for cancer detection[2].

Meanwhile as the field of nanotechnology expands, the possibility of creating miniaturized biosensor devices that are more sensitive, portable and easy-to-use becomes feasible. Nevertheless, it is at this point that we find ourselves facing a challenge, the goals of point-of-care testing (POCT) greatly benefit from the use of label free and real-time detection. For this purpose, we need to be able to successfully analyse samples retrieved directly from the source and without applying any previous purification treatment. The issue is that this implies detecting exceptionally low concentrations of the target molecule against the sample background. This imposes strict conditions for fluorescence-based sensors, as the signal produced by fluorophore labels gets lost in the background noise, thus, impairing the analysis.

A possible solution is to enhance the signal obtained from fluorophores by improving their spectroscopic and photophysical properties, i.e. enhancing the molecular absorption and fluorescence quantum-yield. However, there are intrinsic limitations to this strategy, as the best fluorophores typically have molar absorption coefficients around 10^5 $M^{-1}cm^{-1}$ and fluorescence quantum-yields of almost 100%. A more interesting option is to increase the number of photons in the excitation and emission from a fluorophore and thus increasing the detected fluorescence intensity.

For this purpose, a nano-antenna strategy may be implemented, taking advantage of a physical phenomenon known as the localized surface plasmon resonance (LSPR), which gives rise to strong local electric fields optically-induced using metallic nanoparticles. The apparent photophysical properties

of a fluorophore placed in the regions of enhanced local field can be strongly modified, and it can result in powerful emitted fluorescence signals.

1.1 Nanotechnology

Micro and nanotechnology have drawn a large research interest over the past years. The potential of miniaturizing technologies is almost limitless. In the field of electronics smaller components can mean faster and more complex systems, which have revolutionized the modern way of life.

Furthermore, this can also be applied into other scientific fields, such as biological and medical, by allying the miniaturization of biosensors, which can turn complex and time-consuming laboratorial procedures, into fast and easy to use handheld devices with the discovery of novel detection systems.

Examples of this can be easily spotted, diseases like diabetes can now be monitored easily by the patients, with a small and relatively cheap device. Also, other important medical conditions have now drawn the attention of this technology. With new research data, pinpointing very specific cancer markers, the ability to create new diagnosis machines is within our grasp, like miniaturized optic sensors.

Nonetheless, as in many cases, even though we have the know-how to detect certain molecules, we do not have the technology to achieve the equipment sensitivity necessary for when the target is in a very low concentration. We then, must be able to distinguish the desired signal from the background noise.

Many tactics may be employed, the simpler is to purify the sample to be tested, but this defeats the purpose of point of care testing, which is a label free, fast and easy analysis process to use in a portable device. Other approaches could be improving the photon detection sensitivity or the fluorophore's quantum yield. Considering that the first approach is limited by our current equipment technology and the latter approach is limited since the fluorophores used currently already present high extinction coefficients and quantum yields of almost 100%, a possible solution is to increase the number of photons that can be detected from a fluorescent molecule and, thus, to increase the signal intensity.

So, in order to aid in overcoming this obstacle, a main factor of interest in this project is the real-world application of the technology described previously. For that purpose, it is intended to test the feasibility of a gold nanoparticle 2-D organized array, and test the fluorescence enhancing capabilities of such structure for nucleic acid detection.

1.2 Fluorescence

Discovered in 1845 by Sir Frederik William Herschel[3], fluorescence can be defined as the emission of light by a molecule when it returns to the fundamental state, S_0, having been previously promoted to an excited electronic state.

This excited electronic state is the result of a photon being absorbed by a fluorescent molecule, if the photon meets the Bohr condition, i.e. that the photon energy matches the difference between two energy states of the molecule. The intensity with which the molecule absorbs the photon's energy is measured by the fluorophore's extinction coefficient.

Once in the excited state, this energy can be released by various paths: it can be non-radiatively, such a intersystem conversion or lost through vibration, or; it can be radiatively, such as fluorescence or phosphorescence[4].

The fluorescence phenomenon occurs when, the photon's energy is absorbed, and the molecule is brought to higher excited state it decays through vibrational relaxation or internal conversion (IC) to the lowest vibrational energy state of S_1. From there, the excited molecule decays to S_0 releasing a photon with an energy equal to the difference between those two states. This process has a typical duration of around 1 to 10 nanoseconds[4].

The loss of energy as the molecule relaxes to the lowest vibrational energy state of S_1, from which fluorescence occurs, leads to the energy of the emitted photon being typically lower than the one absorbed, or in other words the wavelength range of the molecule's emission is red-shifted relatively to its absorption. This is a heuristic picture of an interesting phenomenon known as the Stoke's shift. This is an advantage of fluorescence detection, being that the energy provided by the excitation light and the one emitted by the fluorophore do not present overlapping wavelengths, thus facilitating the retrieval of a signal with low background noise, unlike, for instance when analyzing light absorption or scattering at a given wavelength[4]- [6].

As for phosphorescence, it occurs when there is a transition from the excited singlet state manifold to a triplet state, called intersystem conversion (ISC). This phenomenon is characterized by having longer lifetimes than fluorescence, that can range from micro- to milliseconds.

This phenomenon can be illustrated using a Perrin-Jablonski Diagram (Figure 1.1).

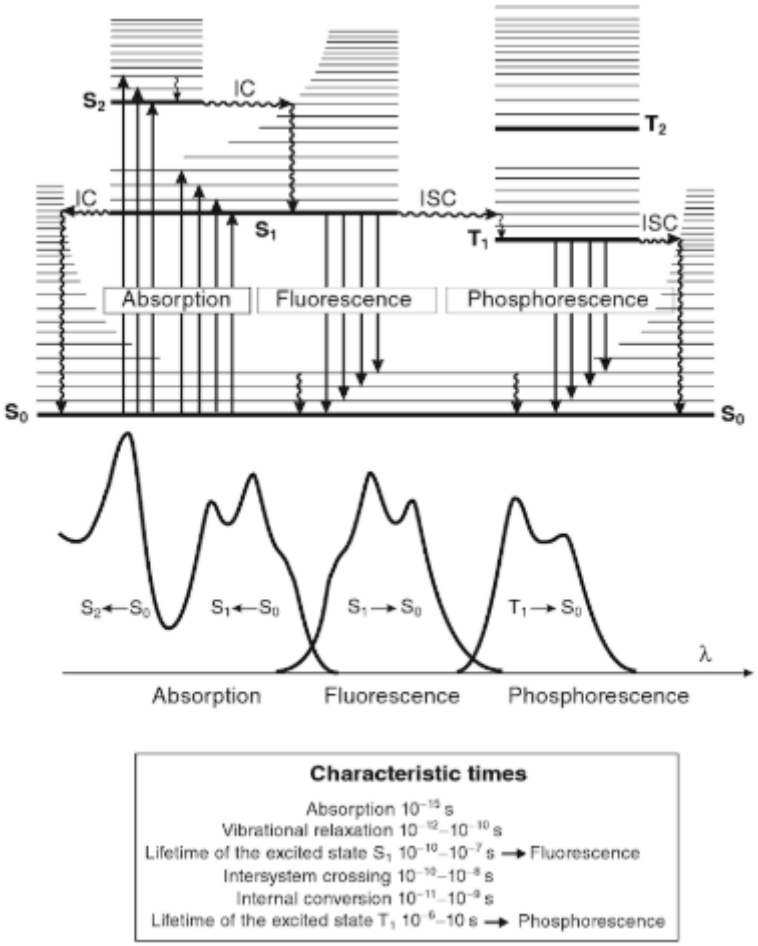

Figure 1.1- Perrin-Jablonski diagram used to depict the phenomenon of absorption, fluorescence and phosphorescence. Difference of wavelength of absorption, fluorescence and phosphorescence and characteristic times of the processes described[4].

By attaching a fluorescent label to a given substance of interest and shinning a light on it, a signal can be detected that indicates the presence of such substance. Furthermore, it can be used to probe changes at the molecular scale due to the sensitivity of emission intensity or lifetime to molecular environment. Fluorescence labelling proved to be a successful technology, being widely used nowadays in life sciences and biotechnology research and development[7].

1.2.1 Fluorescence Quantum-Yield

Some fluorophores emit strongly than others, thus providing more sensitive output readings. This aspect can be quantified by the photophysical property of fluorescence quantum-yield (Φ_F).

It is defined as the ratio between the photons emitted and absorbed by a given fluorophore[8].

$$\Phi_F = \frac{\text{Number of photons emitted}}{\text{Number of photons absorbed}} \qquad \text{Equation 1.1}$$

The maximum yield possible is 1, in other words 100% of the photons absorbed are then emitted by the molecule.

1.2.2 Emission Lifetime

Fluorescence is a transient process, so an important factor to consider is how long a fluorophore remains in the excited state after it has absorbed a photon[5] [6].

Typically, this is a process of 1st order kinetics,

$$n(t) = n_0 e^{-\tau t} \qquad \text{Equation 1.2}$$

Where *n*(*t*) is the number of fluorophore molecules in the excited state at a given time (t) after excitation, n_0 the number of fluorophore molecules in the excited state when the energy pulse is provided and τ is the fluorescence lifetime.

The excited state population is experimentally inferred from the intensity of emitted photons (*I*), and so we can also write equation 2 as follows.

$$I(t) = I_0 e^{-\tau t} \qquad \text{Equation 1.3}$$

The fluorophore's lifetime is by definition related to the radiative and non-radiative decay rates,

$$\tau = \frac{1}{k_r + k_{nr}} \qquad \text{Equation 1.4}$$

1.3 Metal-Enhanced Fluorescence

Based on the discoveries of Drexhage[9] and Lakowicz[5] [6], an extensive field of research rose. The first noticing that fluorophores situated near metallic surfaces presented improved capabilities, useful in detection assays, and the latter by applying these findings to a nanometric scale. The term metal-enhanced fluorescence (MEF) was then created.

The metallic surfaces can interact with the fluorophores in 3 distinct ways:

- Transferring energy from the fluorophore to the metal;
- Modification of the radiative decay rate of the fluorophore;
- Concentration of the local electric field;

The first mechanism dominates at small distances and leads to a loss in energy released as light from the fluorophore. This phenomenon is a non-radiative decay process, and when it prevails then fluorescence quenching is observed, instead of fluorescence enhancement.

The second, occurs due to higher photonic mode density in the proximity of metallic nanostructures, increasing the radiative decay rate of the fluorophore, which will, in turn, contribute to a higher apparent fluorescence quantum yield.

But for this project, the mechanism that is more relevant is the latter, of local field enhancement. Also termed as “antenna” effect, it is known that the electric field is intensified around the edges of metallic structures due to optically excited plasmon oscillations. The surface plasmon resonance (SPR) is responsible for this local field effect, as detailed in chapter 1.3.1. The SPR frequency or peak wavelength depends on the nanoparticle composition, size, shape and environment, and it can be tuned across the visible to near infrared spectral ranges.

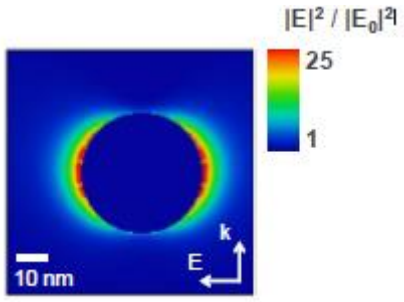

Figure 1.2 - Local electric field enhancement in the adjacent area to a metallic nanoparticle calculated from simulations of discrete dipole approximation[10].

Since the local electric field is amplified, so is the molecular absorption, as the latter scales proportionally to the photon flux, which in turn is proportional to the electric field squared. The fluorescent molecule is excited more often, and this higher probability of promotion to the excited state then increases the number of emitted photons by radiative decay.

$$P_{Fluorophore} = k \times n \times QY \qquad \text{Equation 1.5}$$

$$n \propto |E|^2 \qquad \text{Equation 1.6}$$

In the equations 1.5 and 1.6, $P_{Fluorophore}$ is the fluorescence emitted power, *k* the absorption cross-section of the fluorophore, *n* the photon flux, E stands for the electric field and finally QY is the fluorophore’s quantum-yield.

1.3.1 Surface Plasmon Resonance (SPR)

This phenomenon was first described by Mie in 1908[7], and consists of charge density oscillations, as described in figure 1.3. The model used to explain the SPR, treats the metals as a positively charge matrix of ions and an electron gas moving under the electrostatic potential due to the ions’ attraction. When an external electric field is applied on a metallic structure, the electrons move in the same manner in the material. This displacement of charge causes these electrons then to be attracted to the positively charged ions via a Coulomb’s restoring force. This causes a quick oscillations of charge density in the particle creating an electric field. Most of this energy is dissipated in two ways, first by collisions between electrons, which is very fast (femtosecond timescale), and then by dissipation to the positively charged

lattice and surrounding environment as collective vibrations, i.e. dissipated as heat. So, as long as the particle is irradiated at a wavelength in the spectral range of the SPR, this influx of energy will maintain the plasmon oscillation, but it dissipates almost immediately.

At the nanoscale, it is formed a localized surface plasmon resonance, meaning that the plasmon oscillation is confined by the particle's surface[11].

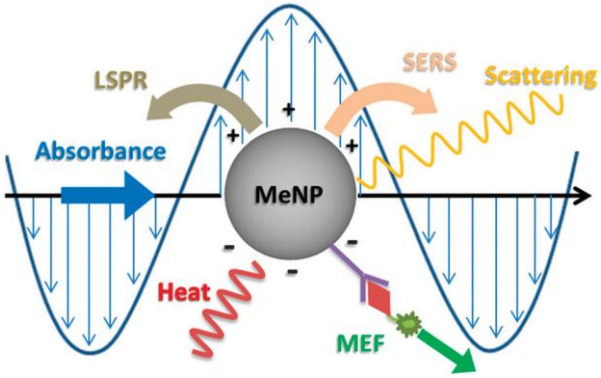

Figure 1.3 - Representation of the induced surface charge oscillations caused by application of an external electric field[11].

Throughout the years many different geometric shapes have been tested, aiming to increase the local field effect and many have proven to be successful. For this project the selected shape was a nanosphere dimer, interspaced by a nanometric distance using DNA spacers. This shape has proven to work in previous research studies[12], with the rationale behind it being the creation of an electric hotspot in the gap between the two spheres (Figure 1.4). This happens for an optically active hybridized plasmon mode in which the oscillations of electrons in both particles are in-phase and oriented along the interparticle axis, also termed longitudinal mode.

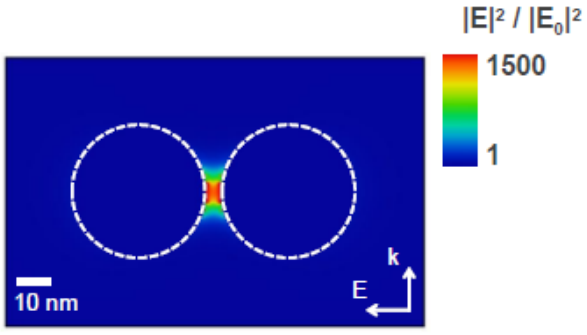

Figure 1.4 - Local electric field amplification in the interstice between two AuNPs[10].

1.3.2 DNA Spacer

As mentioned above, the distance between metallic particle and fluorophore is of extreme importance, because if the distance is too small then emission quenching becomes dominant. However, if they are too far apart the localized surface plasmon will not affect the fluorophore and, therefore, there will be no fluorescence enhancement. In between these two extreme cases, there is an optimum molecule-particle distance for attaining the maximum effect for emission enhancement.

Since in this work the selected geometry is that of an interspaced dimer of nanospheres with a fluorophore located in the gap (hot-spot for emission amplification), the control of such interspace length is crucial. For that DNA strands have been used in the literature to provide adjustable and stable spacer between particles[13]- [15].

These DNA strands have been manufactured to possess a spacer of 10 adenines, as well as a thiol group in the 5' termination, which allows for their attachment onto the gold nanoparticles (AuNPs) used in the project.

By attaching complementary strands to two separate particle sets, it is then possible to drive their assembly into dimers and larger aggregates by allowing the complementary strands on their surfaces to hybridize. It is then possible to control the length of the strands by simply varying the number of nucleotides that compose them, in order to attempt tuning the gap separation.

1.4 Tested compounds

1.4.1 Aluminium Tetrasulfonated Phthalocyanine (AlPcTS)

The fluorescent compound was selected because it was previously studied in the group. Furthermore, it is a very interesting molecule that has shown promise in various areas[16], from infrared sensors[17] to the application in cancer photodynamic therapy[18].

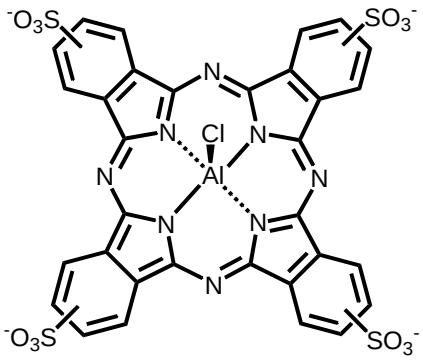

Figure 1.5 - Aluminium tetrasulfonated phtalocyanine chemical structure.

1.4.2 Fluorescently-labelled DNA oligonucleotides

The investigation of fluorescently-labelled oligonucleotides in the research group is currently undergoing with the aim of creating a DNA sensor whose fluorescent signal could be enhanced by the metallic nanostructures used.

The concept of molecular beacon has been described in the literature and presents promising approach to the real-world sensing applications of metal enhanced fluorescence[19]-[22]. The conjugation of molecular beacons with metal nanoparticles has enabled the development of miniaturized biosensors. In the scheme presented in figure 1.6, the mechanism of BF1-BD2-TD is shown(DNA sequences' specifications in annexed tables 6.17-19).

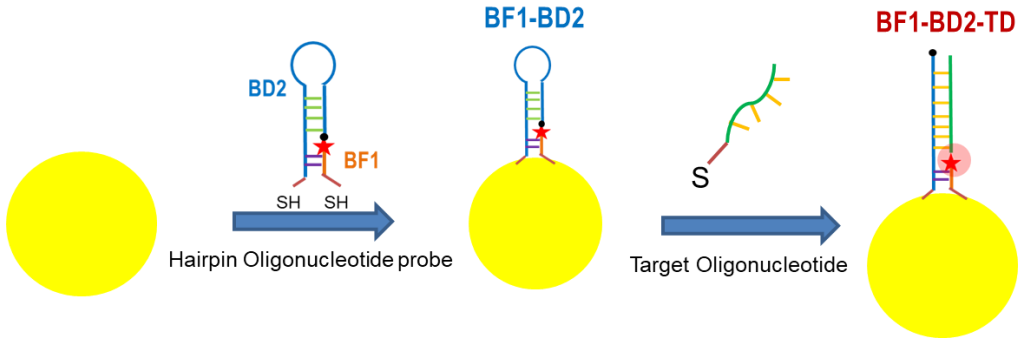

Figure 1.6 – Schematic overview of the molecular beacon action. The thiol groups are shown in (S), the quencher QSY-21 (●) and the fluorophore ATTO-647N dye (★).

As it can be seen in the figure above, when only the probe is present the fluorophore is quenched due to the presence of QSY-21. However, when the target is added, hybridization with the DNA hairpin, changes its conformation and forces the distance between the fluorophore and its quencher to increase, allowing the fluorophore to emit fluorescence. The distance separating the fluorophore and the nanoparticle is rather crucial if plasmon-enhanced fluorescence is sought, since there is an optimum distance to the nanoparticle surface, as previously discussed. This can be controlled with the size of the oligonucleotides used, since when in a double-stranded DNA (dsDNA) conformation this structure is quite rigid and can be assumed to be straight.

The molecular beacon designed at the host laboratory is slightly different from that described in the previous paragraph. Briefly, the molecular beacon is attached to the particle surface by a thiolated oligonucleotide that is 10-bp long and it separates the fluorophore from the metal surface by about 3.4 nm. This distance was previously calculated to be the optimal distance for maximum enhancement of the fluorophore's emission at the tip of a gold nanorod of size 25 nm × 60 nm. In this work, it was mostly studied the fluorescently-labelled oligonucleotide without the hairpin segment of the molecular probe, hereafter named BF1-BT, in order to evaluate the enhancement effect by plasmonic antennas.

For the fluorophore, ATTO-647N dye was chosen, it has been reported to be used in stimulated emission depletion microscopy of living cells, due to its high stability[23]. However, its low polarity can be a disadvantage, since it can strongly stick to glass surfaces, possibly masking the desired signal. On the other hand, it presents a high quantum-yield and an absorption and emission peak of 646nm and 664nm respectively, slightly red-shifted from those of the metallic nanostructures used, making it possible for the MEF to occur[24].

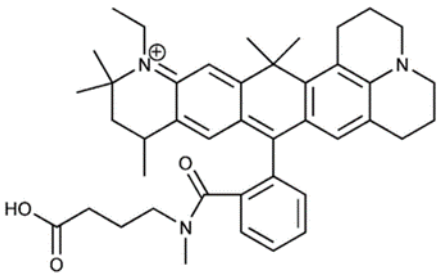

Figure 1.7 – ATTO-647N dye molecular structure.

A great advantage of using sensing strategies like molecular beacons, is the ability to distinguish in a "switch-like" manner if the desired molecule is present in the sample being tested. Moreover, it virtually guarantees that if fluorescent signal increase is obtained, it is due to a positive result, being that it is highly specific and can be made to be less or more stringent, depending on the DNA strands used[19].

1.5 Nanoparticle Film

The promising optical properties demonstrated by coupled metallic nanostructures, such as dimer particles, has prompted the application of these systems in sensors. Nonetheless, some challenges arise because the experiments made to test and report phenomena, such as MEF, are performed in controlled environments, but in a real-life use, the sensors must have an organized array of plasmonic structures over a large surface area, in order to give sensible readouts.

Therefore, if MEF based sensors are to be produced, a method for the construction of organized 2-D nanostructures array over large areas must be developed.

Many different approaches to solve this problem have been taken. While "top-down" approaches, give a more precise control of the nanostructures created[25][26], they are usually expensive and time-consuming. In this work, the focus is on the application of a "bottom-up" approach in order to obtain a large area of structured films.

For instance, the deposition of nanoparticles in microchannels has been reported by functionalizing the surface of the channel with a substance able to attach to itself to the AuNPs and then injecting the NPs at a flow rate which allows for the attachment to the surface but also eliminates any particles not bonded to the surface[27]. This thesis is mainly focused in evaluating the performance of 2D films of nanoparticles for fluorescence enhancement, which could in a later stage be used as plasmonic substrates for microchannels that could find application in a lab-on-a-chip device.

Other techniques, for instance, applying the Langmuir-Blodgett technique have also been reported[28]-[30]. In this approach, a layer of nanoparticles is set on a liquid-air interface and then a plate perpendicular to the surface, rises slowly from the solution, transferring the AuNPs to the solid substrate in the same orderly fashion as they are present in the solution interface. An advancement of this approach for nanoparticle dispersion is the use of an electro-spray to deposit the nanoparticles in the liquid-air interface, thus, avoiding clustering of particles and allowing for a more compact and 2D organized layer. This happens because the droplets formed by the electrospray are so small that upon reaching the interface they gently deposit, without penetrating the sub-phase nor creating any turbulence that could disrupt the organized array[31].

However, before attempting more technologically challenging techniques, a basic approach was taken of deposition by drop-casting[32] [33]. This approach consists of depositing a droplet containing AuNPs in a surface and as it dries an array of nanoparticles is formed.

However the direct evaporation from the water-based dispersion of nanoparticles can lead to the deposition of clusters or multilayers of AuNPs, which is not desired, so for avoiding that the protocol implemented was based on Liebig,*et al.*[34]. By adding an ethanol-toluene mixture to the droplet a compact organized layer of AuNPs is formed in the air-liquid interface and as the droplet dries, this layer

is slowly deposited onto the surface, thus creating an organized array and minimizing the stacking of AuNPs.

1.6 Confocal Fluorescence Microscopy

This method gets its name from the superimposition of two focal volumes used to define the observation volume. The light is focused onto the sample by a lens or objective and then the sample's emission is spatially selected by removing the out of focus light using a pinhole filter. A filter is also used to select a window of wavelength correspondent to the fluorescence emitted by the sample while cutting off the excitation light wavelength.

The emission signal is then collected by highly sensitive photodetectors and digitalized. The CFM used also allows for time-resolved fluorescence measurements in the nanosecond timescale by means of Time-Correlated Single Photon Counting (TCSPC). Briefly, it consists of using a pulsed laser source for instantaneous sample excitation and then detecting the first photon arriving at the photodiode detector. By keeping record of the time interval between the pulse and the photon arrival at the detector and repeating this operation over many excitation cycles at a low detection rate, a photon arrival histogram can be constructed, which is the fluorescence decay measured for a sample.

In contrast to commonly used wide-field microscopes, in CFM only one surface position, or diffraction-limited spot, is illuminated at each time. This allows for a better resolution, but results in a longer imaging time necessary to scan the area of the sample. Nevertheless, this is but a small setback compared to the potentialities of this technique.

1.6.1 Fluorescence Correlation Microscopy (FCS)

This technique allows to gather data on a compound's properties, be it dynamic, such as the diffusion coefficient, or optical, like the brightness of an individual molecule. It requires a previous characterization of the volume and shape of the microscope's observation volume. Then, it becomes possible to calculate properties of the sample compound, by measuring the fluctuations of fluorescent signal as the molecules diffuse through that observation volume[35]- [37].

This technique has found widespread use in multiple research fields, allowing, for instance, the study of single-molecule properties, such as molecular diffusion or binding and reaction kinetics[37].

In this work, this technique was used for various purposes: determination of diffusion coefficients and evaluation of enhancement factors and of individual molecule brightness.

2. Materials and Methods

2.1 Reagents

All glass materials used in the experiments were washed with RBS 5% detergent and rinsed thoroughly with mili-Q water.

11-Amino-1-undecanethiol hydrochloride (AUT) (HSCH2(CH2)9CH2NH2·HCl, ≥99%, Sigma-Aldrich); 11-Mercaptoundecanoic acid, (HS(CH2)10CO2H, ≥98%, Sigma-Aldrich); (3-Mercaptopropyl)trimethoxysilane (HS(CH2)3Si(OCH3)3, ≥95%, Sigma-Aldrich); Agarose (Nzytech); ATTO655-COOH (ATTO-Tec); Bis(p-sulfonatophenyl)phenylphosphine dihydrate dipotassium salt (BSPP) (C18H13K2O6PS2·2H2O, ≥97%, Sigma-Aldrich); Boric Acid (H3BO3, ≥99,5%, Sigma-Aldrich); EDTA (C10H22N4O8·H2O, ≥98,0%, TCI Chemicals); Ethanol (≥99,8%, Panreac); Ethanol absolute for UV, IR, HPLC (C2H6O, ≥99,9% , AppliChem); Glicerol (C3H8O3, 99,5%, Sigma-Aldrich); DNA strands (SA15, PA15, PAF30, SAF30, BF1-BT and BF1-BD2-TD molecular beacon, STABvida); Glass slides for Confocal Fluorescence Microscopy (1000D, Ø=22mm, Menzel-Gläser, Thermo-Scientific); Gold Nanoparticles: 80,40 and 20nm(Nanopartz); Gold Nanorods 25-650 (Nanopartz); Hydrochloric Acid (HCl, ≥36,5%, Sigma-Aldrich); PBS (in tablets, pH 7,4, 0,01 M de phosphate buffer, 0,027 M de KCl e 0,137 M de NaCl para 200 mL, Sigma-Aldrich); RBS 50 (Fluka); Sodium Chloride (NaCl, ≥99,5%, Sigma-Aldrich); Sodium Citrate Tribasic Dihydrate (Na3C6H5O7·2H2O, ≥99,5%, Sigma-Aldrich); Sodium Hydroxide (NaOH, ≥98,0%, Sigma-Aldrich); Sulfuric acid 96% (H2SO4, Carlo Ebra); Toluene (C7H8, ≥99.8%, Merck); Trizma® base (C4O3H11N, ≥99,5%, Sigma-Aldrich).

2.2 AuNPs Dimer Manufacturing Protocol

For this experiment the nanoparticles were firstly functionalized with the DNA strands and after hybridized to form dimers, as shown in figure 2.8.

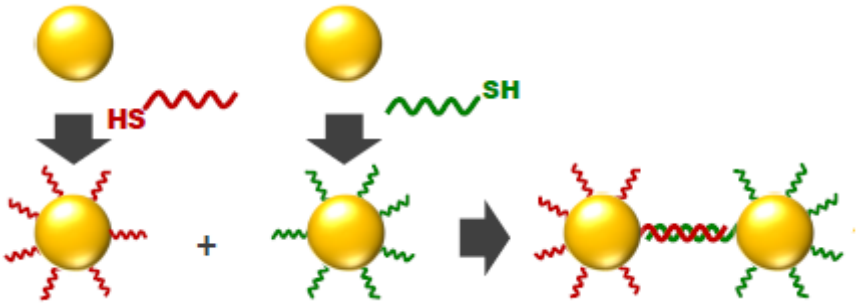

Figure 2.8 - Schematic representation of AuNPs spacing using DNA spacers[1].

DNA strands, with 15 nucleotides (nt) (PA15 and SA15) were used to functionalize the AuNPs. Each single strand DNA is composed of the nucleotides and in the 5' end by a 10 adenine spacer and also a thiol C6 group, to allow the DNA to bind to the NPs (specifications are present in tables 6.13 and 6.14 of the annexes). The NPs tested were of 80nm in diameter (more information present in the annexes, Table 6.12).

The selected method for the dimerization protocol was to first functionalize the NPs individually, with the DNA strands. The concentration of DNA strands in the solution was calculated based on the theorical maximum loading capacity of each size nanoparticle[38] with an excess of 10 times. Then to incubate the two samples together allowing for the hybridization of the complementary DNA strands. The AuNPs and DNA were previously treated with Tris(2-carboxyethyl) phosphine hydrochloride (TCEP) [15] and Bis(p -Sulfonatophenyl) phenylphosphine (BSPP) [39] to improve the stability of the DNA and AuNPs respectively, both at a concentration of 1mM. The stock AuNPs are then concentrated from 1000 to 64µL by centrifugation. 8µL of DNA solution are then added to achieve the necessary concentration of DNA. 2µL of citrate buffer at pH=3, with a desired salt concentration (table 2.1 and 3.4) are added in intervals of 10 minutes, until the final volume of 80µL is reached. The solution is then incubated for 1 hour at room temperature to allow the DNA functionalization of the AuNP surface. After, the solution is washed with TBE 0,5x in order to diminish the salt concentration and thus stop the functionalization. At this point the AuNPs should be rather stable due to the negative surface charge of the DNA functionalization, which inhibits aggregation. Part of the solutions containing the complementary DNA strands functionalized AuNPs are mixed in the presence of TBE 0,5x with the desired salt concentration and incubated at the melting temperature for the DNA strands used, for 20 minutes. This enables the hybridization of the complementary DNA strands and therefore creates AuNPs dimers spaced by the double strand DNA (more information on the buffers used present in annex 6.3).

2.3 Separation and characterization of dimers and other agglomerates formed

2.3.1 Agarose gel electrophoresis

To separate the different structures that result from the dimerization protocol, agarose gel electrophoresis was used, in order to separate by size and weight.

A gel with a 0,7% agarose concentration was prepared in TBE 0,5x buffer. The samples were then loaded onto the gel, adding glycerol to help the samples to sediment in the wells. Both the dimerized and the functionalized nanoparticles were loaded, this latter to serve as control for the migration of single functionalized NPs. The electrophoresis was then performed at 110V for 30 minutes, in a VWR chamber and with a power supply EPS 301 from GE Healthcare Life Sciences.

The samples were then extracted from the gel and stored at 5^{o}C in 700µL TBE 0,5x.

2.3.2 UV/Visible Spectroscopy

To determine absorbance spectrum the samples originated from the dimer formation protocol were analysed in a UV/Vis Perkin-Elmer Lambda 35 spectrometer. Spectra for the stock nanoparticle were also obtained using this method. Also, further UV/Vis emission spectra were obtained using the spectrometer attached to the CFM (2.3.4).

2.3.3 Transmission Electron Microscopy (TEM)

Being a crucial tool for observation of nanostructures, this technique allows to see the individual structures of AuNPs. By passing a beam of electrons through the substrate and focusing the data obtained into an imaging device, it is possible to observe the details of that sample being analysed.

Using this technology, it is expected to analyse the efficiency of the dimerization protocol, by comparing the number of dimerized and non-dimerized structures.

For the measurements performed here an electronic transmission microscope HITACHI H-8100 was used, coupled with a ThermoNoran EDS (Energy Dispersive X-ray Spectroscopy) detector and a digital image acquisition.

2.3.4 Confocal Fluorescence Microscopy (CFM)

For this experiment the confocal microscopy microscope used was MicroTime 200 by PicoQuant GmbH. The excitation wavelengths of 482nm (LDH 485, PicoQuant) and 639 nm (LDH 635-b, PicoQuant) are performed by a laser with a pulse repetition rate of 40 and 20 MHz respectively. This is attached to an inverted optical microscope Olympus IX-71. The laser light is focused by a 60x water immersion lens with a numerical aperture of 1,2 (UPLSAPO 60XW, Olympus). The fluorescence emitted by the sample passes through a dichroic mirror specific for the wavelength of laser in use, an emission filter (510ALP (Omega) for the 482nm laser and a 695AF55 (Omega) for the (639nm laser). The light then passes through a 50/50 polarizer beam splitter and is detected by two photodetectors SPAD (SPCM-AQR da PerkinElmer). This signal is then processed by a TimeHarp 200 TCSPC (Time-Correlated Single Photon Counting) by PicoQuant.

The system also contains an attached spectrometer (QE Pro, Ocean Optics) and a charge-coupled device camera (ZC-F10C2, GANZ).

A scheme of the microscope's setup is present in figure 2.9.

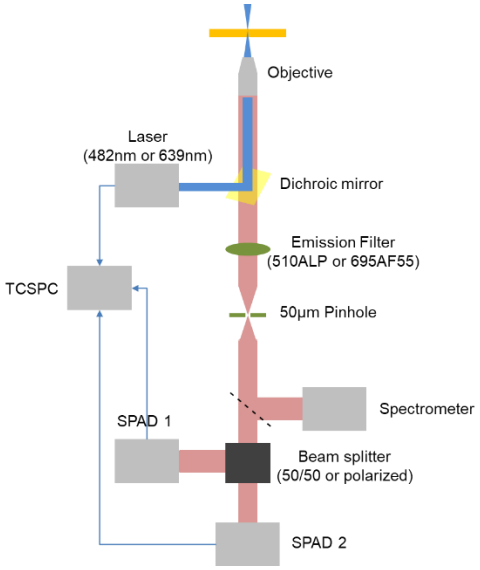

Figure 2.9 – Scheme of the CFM setup.

2.3.4.1 FCS measurements

In order to identify the diffusion time of each sample collected from the dimerization protocol, FCS measures were made. For this a calibration of the detection volume is required. To do so, the molecule fluorescein was used as standard, since its diffusion coefficient (*D*) is known (426μm²/s) [40]. These measurements are taken ~10μm above the slide's surface and for 180 seconds to increase the signal-noise ratio.

The autocorrelation functions were then adjusted using a one species pure diffusion model ($G_d(\tau)$), the expression is given by equation 2.7.

$$Gd(\tau) = \frac{1}{N}\left(1+\frac{\tau}{\tau d}\right)^{-1} \times \left(1+\frac{\tau}{(k\times\tau d)}\right)^{-\frac{1}{2}} \qquad \text{Equation 2.7}$$

Where τd is the diffusion time of a molecule through the confocal volume, N the average number of molecules present in the detection volume, k a geometrical factor describing the shape of the confocal volume through the multiplication of $z0$, the longitudinal dimension and $w0$ the lateral dimension[41] [42].

This can then be correlated with the diffusion coefficient:

$$D = \frac{w_0^2}{4\tau d} \qquad \text{Equation 2.8}$$

The effective detection volume can then be calculated:

$$v_{eff} = \pi^{3/2} \times w_0^2 \times z_0 \qquad \text{Equation 2.9}$$

One important aspect to keep in mind, is the necessity of correlating the data obtained by the two detectors, since after detecting a photon the detector then emits an electronic pulse, known as after pulsing, which, if the signal from the two detectors is not correlated results in a false reading of another photon.

Knowing the characteristics of the observational volume a number of data on a selected molecule can then be calculated, as described in 1.6.1.

In this case the measurements were taken using the 482nm laser, for 30 seconds, with an intensity of 6,7kW/cm².

2.3.5 Glass slides preparation for CFM

Prior to their use in the experiments, the slides were thoroughly cleaned. Firstly, by being rinsed abundantly with water and then with ethanol. Once dried the slides were exposed to UV/Ozone (PSD-UV3 Digital UV Ozone System, Novascan) for 60 minutes. They were then stored in a Petri dish until their use.

2.3.6 Nanoparticle and nanorod sample deposition in glass slides

The clean slides described in 2.2.1, were then exposed to a solution of 1M hydrochloric acid for 30 minutes, after they were abundantly rinsed with water and immersed in mili-Q water solution and sonicated for 10 minutes and dried. Following this, the slides were placed in a methanol solution which was sonicated for another 10 minutes, after this the slides were dried.

The surface of the glass slides was then silanized, by being immersed in a 5% v/v solution of (3-mercaptopropyl) trimethoxysilane in ethanol for 25 minutes. This step helps the nanostructures adhere

to the glass surface, since the thiol groups left in the surface due to this process have high affinity for the metallic structures. The slides were finally rinsed with ethanol, sonicated in methanol and dried.
The deposition of the samples in the surfaces was performed by dropcasting, the drop being removed from the surface after 20 minutes of deposition.

2.4 Further attempts at AuNPs dimerization

For these experiments AuNPs with sizes of 20, 40 and 80nm (more information present in annexes, tables 6.10, 6.11 and 6.12) in diameter were used (structure present in annexes, tables 6.15 and 6.16). The DNA strands used to functionalize and for the subsequent hybridization were PAF30 and SAF30 (structure present in annexes, tables 6.15 and 6.16).

Table 2.1 – Dimerization protocol conditions.

Nanoparticle	AuNP concentration (μM)	[Salt] (mM) Functionalization	[Salt] (mM) Hybridization
20nm Diameter	1,4E-2	70	70
40nm Diameter	1,74E-3	70	70
280nm Diameter	2,66E-4	70	70

The FCS measurements were then performed as described in 2.3.4.1.

2.5 DNA strand coverage of AuNPs

Nanoparticles with sizes of 20,40 and 80nm, were functionalized with DNA strand PA30F or SA30F (consisting of a PA30 or SA30 DNA strand, modified with a molecule of fluorescein at the 3' end), using the same protocol as described in 2.2. For each sample, 12μL of the AuNPs-DNA sample was diluted in 1176μL of TBE 0,5x and its absorption spectrum was viewed using UV/Visible Perkin-Elmer Lambda 35 spectrometer. Also, the sample's emission spectrum was measured with a fluorimeter Fluorolog Horiba Jobin Yvon using various excitation energies of 470,480 or 510nm to measure the spectrum starting at 480,490 and 520nm respectively, for a 2nm slit opening.
Following this, the protocol of Demers, *et al*[43], using mercaptoethanol, was applied, adding this compound into the diluted sample to a final concentration of 20mM. It was then incubated for 6 hours at 37ºC, the sample was centrifugated at 6000rpm for 15 minutes and part of the supernatant was then collected. The emission spectrum of the resulting supernatants was then observed in the same conditions as those mentioned above.
To be able to correlate the data obtained with a concentration of the fluorophore in the sample, a calibration curve of the DNA attached fluorophore's concentration was prepared for in the same conditions as the measurements of the samples was made (present in annex 6.3).

2.6 Analysis of fluorescence enhancement experiments

In order to calculate the maximum enhancement factors, some data must be known, the maximum intensity produced by the burst of fluorescence caused by the fluorophores passing through the observational volume, the background intensity produced by the nanostructures themselves and the brightness of an individual molecule of the fluorophore under non-enhancing conditions, as shown by equation 2.10.

2.6.1 Non-enhanced brightness of individual molecule

This can be calculated using the formula below.

$$\text{Individual NH brightness} = \frac{Average\ intensity}{Average\ number\ of\ molecules} \qquad \text{equation 2.10}$$

In this case, the non-enhanced intensity (δ) of the fluorescent molecules used, was previously calculated by the research group in which this work was developed. This is done by, after calibrating the observational volume, taking FCS measurements of solutions containing the fluorescent molecules desired, then through an autocorrelation curve of the results obtained the average number of molecules in the observational volume can be known. Then to calculate the average intensity measured a gaussian curve can be adjusted to the intensity frequency histogram.

This method can be applied for specific energy excitation, such is the case of AlPcTS or a range of individual brightness can be obtained by testing using different excitation energies and subsequently a linear fitting can be applied that allows for the calculation of the individual non-enhance brightness at a desired wavelength, as long as the excitation power is below optical saturation and pile-up limits.

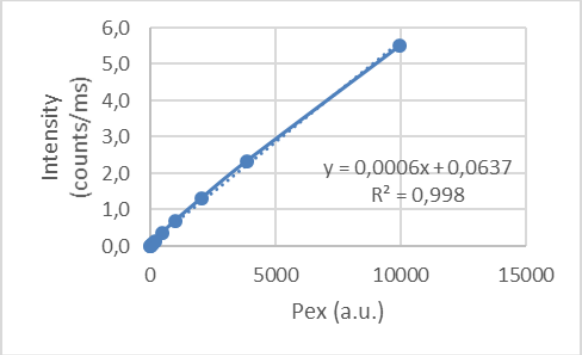

Figure 2.10 – Example of the linear fit used to calculate the individual molecule brightness at a given excitation intensity for BF1-BT.

2.6.2 Background intensity calculation

This data is crucial, for a correct measurement of the maximum intensity of enhanced fluorescence bursts obtained during the experiments. Allowing to subtract the average number of counts produced by the nanostructures, number which can be known by adjusting a gaussian curve to the peak of the intensity frequency histogram. Also, by applying the method proposed in Zhang, *et al.* [44], a threshold can be calculated, to discriminate intense events of enhanced single-molecule fluorescence. For that, the intensity threshold is considered to be μ+6σ, where μ is the average background signal and σ is the standard deviation.

2.6.3 Analysis of maximum intensity bursts by “cherry-picking”

This method consists of choosing the highest intensity producing individual burst obtained in the intensity frequency histogram of fluorescence enhancement experiments. Even though this method can be biased by rare events of extreme emission intensity that are not representative of the average sample behaviour, it has been shown that this analysis produces similar results to that of other methods as the one presented below[45].

This method is best suited for when there is no clear tail for the intensity frequency histogram, but bursts with intensities greatly superior to the average exist.

2.6.4 Analysis of maximum intensity bursts by extrapolation

This method is only applicable in certain cases, since it is based on a tail fit of the intensity frequency histogram, and for that a tail must present a slope to which a fit can be performed. This method gives us not the experimentally obtained maximum intensity but the most probable maximum when considering the dispersion of points of enhanced fluorescence present in the intensity frequency histogram's tail.

2.6.5 Calculation of the maximum enhancement factor

Analysing the MCS traces obtained from the fluorescence enhancement experiments, it is possible to calculate the maximum enhancement factor for the molecules used[44].

The equation 2.11 describes the calculation of ξMax.

$$\xi\mathrm{Max} = \frac{Maximum\ burst\ intensity - Background\ intensity}{\delta} \qquad \text{Equation 2.11}$$

So, to be able to calculate it, one must know the maximum burst intensity, which can be discovered by "cherry-picking" the highest intensity burst in the sample's MCS trace or by extrapolating the maximum possible intensity adjusting a tail fit to the intensity frequency histogram, as described previously. The background intensity is known by adjusting a gaussian curve to the peak of the intensity frequency histogram.

In order to, compare the enhancement factors within different fluorescent compounds the maximum enhancement factor must be normalized, according to the definition of a figure-of-merit, FOM_{enh}[46]. This is accomplished by multiplying it by the fluorescence quantum yield of the compound.

$$\mathrm{FOM_{enh}} = \frac{Maximum\ burst\ intensity - Background\ intensity}{\delta} \times \phi_F \qquad \text{Equation 2.10}$$

2.7 Fluorescence enhancement experiments with single AuNRs

2.7.1 Fluorescence enhancement of AlPcTS by AuNRs

In order to assess the fluorescence enhancing capabilities of metallic structures, assays with aluminium tetrasulfonated phthalocyanine and gold nanorods were conducted.

The nanorods presented dimensions of 25nm of height and 71nm of length and were deposited onto a silanized glass surface prepared as described in 2.2.1 and 2.2.2 and coated with AUT.

Using the 639nm laser, FLIM images were then taken with an energy of 22,2kW/cm^2. As for the FCS measures, these were obtained for 30 seconds with an energy of 0,4 kW/cm^2.

After the addition of the fluorophore, another FLIM image was taken to assure that the area observed remain the same. FCS measures were then taken again, in similar conditions as before, the only difference being that the detection time was increased to 60 seconds.

The AuNRs with most promising MCS traces were selected to further analysis, which was conducted using the "cherry-picking" method described in 2.4.3.

2.7.2 Fluorescence enhancement of BF1-BT by AuNRs

For this experiment, the AuNRs were deposited onto a glass surface prepared as described in 2.2.1 and 2.2.2. Emission spectra were then taken with the 482nm laser with an energy of 34,2kW/cm^2, using the spectrometer attached to the CFM.

A switch to the 639nm laser, and a FLIM image at 2,2 kW/cm^2 was taken to assure that the area of study was maintained. FCS measurements of the AuNRs were performed with an energy of 1,7 kW/cm^2 for 30 seconds to ensure that there were no intensity fluctuations in the MCS traces. Upon addition of the molecular beacon BF1-BT with a concentration of 10nM and an incubation period of 1 hour, the FCS traces of the same AuNRs were measured again, now for 60 seconds. As before the most promising MCS traces were selected to be analysed. In this case they were analysed by the cherry-picking and the extrapolation method.

Also, FCS traces with varying laser intensity of 0,9 kW/cm^2, 1,7 kW/cm^2, 2,6 kW/cm^2, 3,5 kW/cm^2 and 4,4 kW/cm^2 were obtained.

2.8 Nanoparticle 2-D organized layer

As mentioned previously (chapter 1.5), there are several approaches to the creation of 2-D organized nanoparticle layers, but the one chosen was to use an ethanol-toluene mixture to create an organized layer of nanoparticles in the liquid-air interface of a droplet. The ethanol and toluene used, are of spectroscopic grade.

The deposition protocol performed in a glass slide (prepared as described in 2.2.1 and 2.2.2), comprised a 100µL drop of solution containing nanoparticles simply concentrated 7 times from the stock solution being deposited in the glass slide. Then an ethanol-toluene solution in a ratio of 5:1 was added to the droplet with an Hamilton syringe, to a ratio of 1:0,4 between the droplet and the ethanol-toluene mixture[34]. The droplet is then left to dry.

A schematic illustration of the method is presented below.

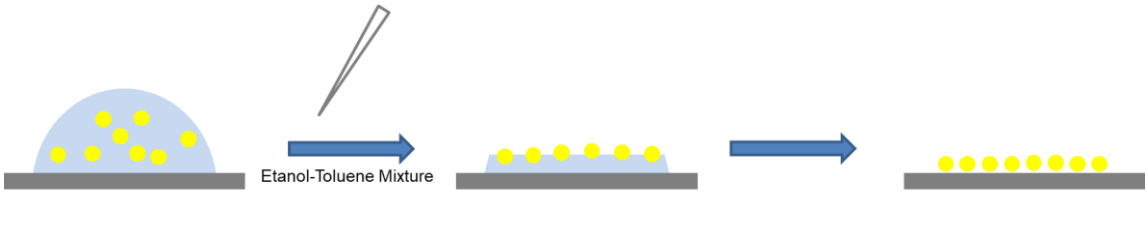

Figure 2.11 - Simplified illustration of film-casting and monolayer formation after the addition the ethanol–toluene mixture.

The experiment was performed with nanoparticles of 20,40 and 80nm of diameter.

2.8.1 CFM analysis of the 2-D nanoparticle layers

To understand the structure of the prepared layers, the slides were observed using CFM, with the aid of the attached optical microscope. In order to characterise the surface, emission spectra of multiple points were obtained for different structures in the layers, as well as CFM and optical microscope images.

2.8.2 Scannig Electron Microscopy (SEM) analysis of the 2-D nanoparticle layers

In order to obtain a more exact comprehension of the deposition's morphology, scanning electron microscopy was used. With this technology, an image of the nanoparticles can actually be formed, by analysing the interactions of the electron beam with the atoms present in the sample, and since the wavelength of this beam is much smaller than that of light, it is possible to perceive details of much smaller structures.

The JEOL JSM-7001F Field Emission Scanning Microscope was used, operating at high vacuum. The samples were laid in a carbon support and covered by a gold film and measured after it dried.

2.8.3 Fluorescence enhancement of BF1-BT in 2-D nanoparticle layers

The experimental setup is similar to that of previous experiences, however in this case the fluorescent enhancing structures will be the nanoparticles organized in a 2-D array following the experiment of 2.7.2. For this case the surface composed of nanoparticles of 80nm of diameter was chosen.

2.8.4 Fluorescence enhancement of BF1-BD2-BT in 2-D nanoparticle layers

To test the action mechanism of BF1-BD2-BT, a surface with 80nm diameter AuNPs film obtained was used. FLIM images were then taken using the 639nm laser with an excitation power of 1,7 kW/cm^2.

3. Results and Discussion

3.1AuNPs dimer synthesis

Ever since the implementation of DNA strands as spacers, there has been an attempt to optimize this protocol. The AuNPs are originally citrate-stabilized, which confers them negative surface charge thus preventing aggregation by electrostatic repulsion between them. Since the DNA strands are negatively charged as well, when adding them to a solution with AuNPs stabilized in citrate, the surface repulsion inhibits the thiol attachment of the DNA strands. To overcome this, salt is added to the solution, in order to screen charge repulsion and enable the DNA strands to approach the AuNPs and react with their surface for particle functionalization.

Even though this method has proven successful, it has some inherent problems: the addition of salt and subsequent charge balancing can lead to the aggregation of NPs. Furthermore, as the DNA strands start to cover the NP's surface, the surface charge starts becoming more negative and thus repulsive forces towards other DNA chains increase, preventing their addition.

Hence, a delicate balance of salt must be achieved to functionalize NPs surface effectively. This proved to be a challenge with initial protocols using a faulty and lengthy salt-aging process, until Xu Zhang[15], published a protocol of salt addition at low pH (pH=3), thus facilitating the control of the surface charge of the particle, and increasing the efficiency of the procedure.

The particle dimerization protocol was optimized in order to overcome problems of particle aggregation, probably due to variations in supplied particle batches. The use of BSPP instead of citrate aimed to improve AuNPs stability at the beginning of the protocol[39]. As for the DNA strands, since they had been stored for some time, the addition of TCEP was introduced to remove any disulphide bonds present in the stock DNA strands, which could impede the AuNP functionalization[47]. Another aspect optimized in this experiment was the salt concentration applied to the samples during functionalization and dimerization, that were chosen to be 200 mM and between 60-80 mM, respectively.

The most promising samples were used to perform further optimizations of sample preparation. In the table 3.2 their specifications are present, as well as their denomination to be used throughout this document.

Table 3.2 – Specification of the main alterations performed on the basic protocol.

Sample	Functionalization Salt Concentration (mM)	Dimerization Salt Concentration (mM)	Denomination
A	200	80	A1
A	200	60	A2
B	200	80	B1
B	200	60	B2

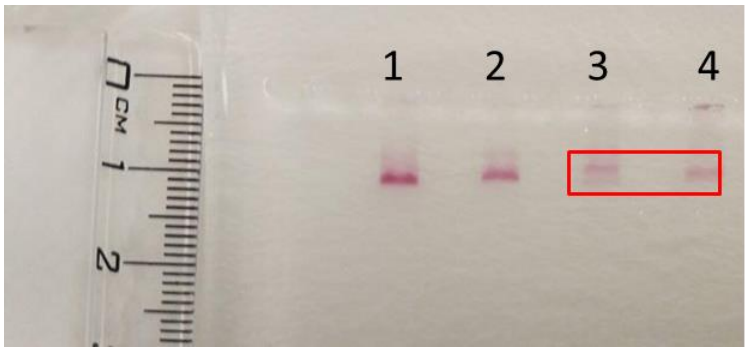

Figure 3.12 - Purification of samples A, trough electrophoresis. AuNPs functionalized with the DNA chains PA 15 and SA 15, present in lane 1 and 2 respectively. Samples A1 and A2 in lanes 3 and 4 respectively.

The bands present in the gel are identified from the bottom up, being that in the image above the bottom band present in lane 3 is identified as A1-b1, the next band is A1-b2, and so on, with this nomenclature being applied to sample identification from now onwards.

In lanes 3 and 4 of figure 3.12, two bands are highlighted in red, which are observed in each lane and appear to be aligned. This shorter migration distance in the gel indicates the presence of larger structures that were later confirmed to be dimers of functionalized AuNPs. The purification of samples B showed similar results, which gave support to the interpretation of gel results.

3.1.1 CFM coupled with UV/Vis spectroscopy

Early attempts to produce NP dimers had demonstrated difficulties in applying the previously optimized protocols successfully. So, before any microscopy measurements, the absorption spectra of the nanoparticles as supplied were measured in order to be able to compare it to the sample's specification[48]. Furthermore, these measurements allowed assessing if the use of BSPP improved or not the AuNPs' stability.

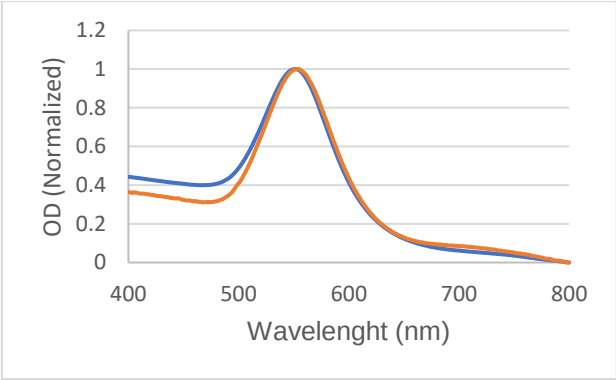

Figure 3.13 - Normalized absorption spectrum for stock (blue) and BSPP treated (orange) 80nm diameter AuNPs.

The maximum absorption is at the expected wavelength, around 550nm, but there is also absorption feature around 750nm, that indicates the presence of NPs aggregates. Interparticle coupling in aggregated particles induces a red-shift of the absorption maximum, or even the appearance of another band deviated to the red/infrared range of the spectrum[48]. This evidence for particle aggregation could explain the lack of stability even when BSPP is added, because no change was observed in the red-

shifted feature of the spectrum. So, the stabilizing effect of BSPP was not enough to solve the aggregation problem of the AuNPs used in this study.

TCEP was also used to optimize the particle dimerization protocol. As described in the literature, its use allows for the removal of small alkanethiol molecules, which may cap the DNA strands. By adding TCEP the disulphide bond is cleaved, which increases the availability of the thiol group in the DNA strands for reaction with metal surfaces[15].

The combined use of BSPP and TCEP additives allowed to prepare samples of single and dimerized AuNPs and their optical spectra were characterized by CFM using a low level light spectrometer with sensitivity for individual particles. The particle sample was deposited from solution onto a glass slide and individual particles were identified from images of optical microscopy (CFM) – see figure 3.14.

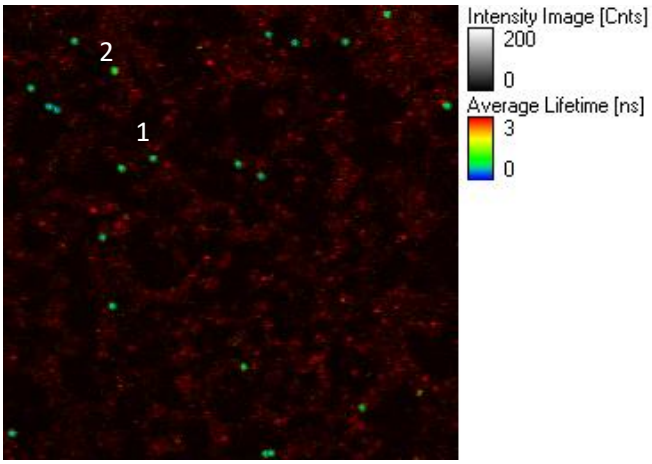

Figure 3.14 - Image obtained through CFM of sample B2-b2. Examples of diffraction-limited spots showing photoluminescence spectrum of single and dimerized AuNPs are identified as 1 and 2, respectively.

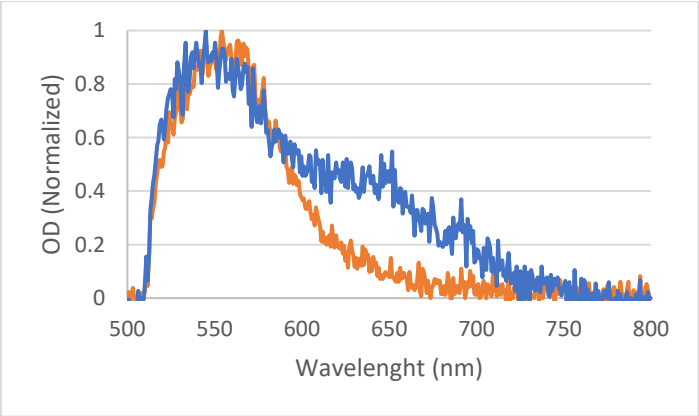

Figure 3.15 - Normalized extinction spectrum for functionalized AuNPs (orange) and dimerized AuNPs (blue) of sample B2-b2.

As expected, the spectrum changes for the dimerized AuNPs, as it shows a second band, or shoulder, around the 650nm range due to the longitudinally-coupled plasmon mode[48]. Other emission spots in figure 3.14 were also measured and showed an emission spectrum of either single or dimerized AuNPs. This indicates that dimers are present in the sample, nevertheless this could be the result of

spontaneous aggregation. In order to dismiss this hypothesis, the dimer samples were characterized by electron microscopy.

3.1.2 Transmission Electron Microscopy (TEM)

By depositing the samples in TEM grid, it is possible to infer about sample composition from the images of the nanostructures present in there. The first band of the gel (e.g. A2-b1) shows essentially single particles, while the second band (e.g. A2-b2) shows many dimer objects (see figure 3.16). These results confirmed the interpretation of the gel, as previously discussed.

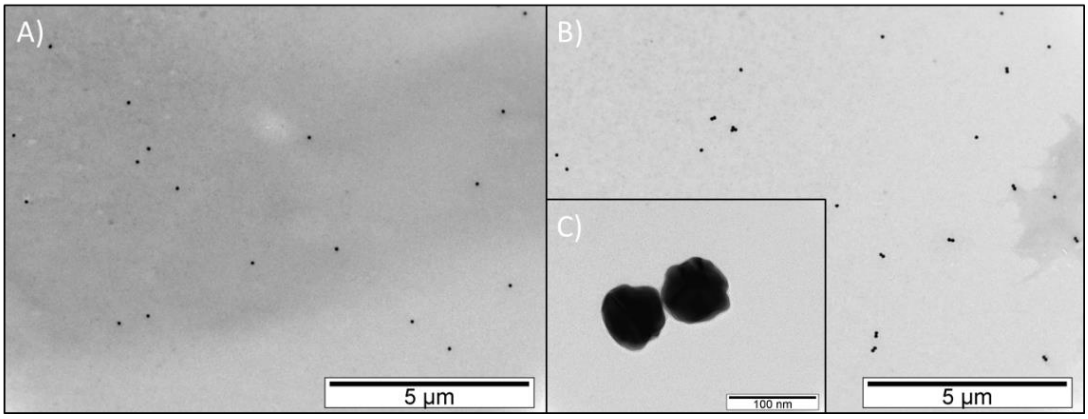

Figure 3.16 - Image obtained by TEM of sample A2. Image A) and B) correspond to A2-b1 and A2-b2 respectively. Image C) is a magnification of image B).

A count of the different structures present in each sample was performed, to assess the percentage of dimers present.

Table 3.3 – Percentage of dimers present in the samples analysed by TEM.

Sample	Percentage of dimers (%)
A1-b1	5,7
A1-b2	49,1
A2-b1	0
A2-b2	49,6
B2-b1	6,1
B2-b2	63,9

The results shown in table 3.3 are in accordance with expected results, namely that the bands with dimers should migrate slower, through the agarose gel, than those the single AuNPs.

However, even though it is possible to observe a significant increase in the occurrence of dimerized structures, the efficiency of dimer formation should be higher. This deviation from the expected results, may have been caused by the low stability and subsequent aggregation of the stock AuNPs. Seldomly, it was observed the retention of aggregated particles in the loading well of the gel. Nevertheless, these results show that it was possible to achieve particle dimerization, as desired.

3.1.3 FCS measurements of DNA-functionalized AuNPs

Single or dimerized AuNPs have different size and shape and, in principle, these differences could be discriminated by FCS measurements in solution that give information on their transport properties, e.g. diffusion coefficient.

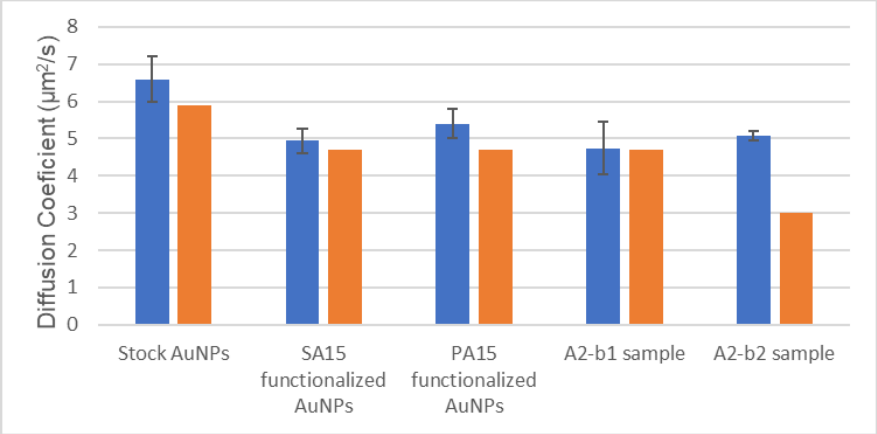

Figure 3.17 - Diffusion coefficients obtained for stock AuNPs, AuNPs functionalized with SA15 or PA15 DNA strands AuNPs, sample A2-b1 and sample A2-b2, using CFM in blue. Estimated diffusion coefficient values for each sample are present near the sample's coefficient in orange.

Analysing the diffusion coefficients of the several samples, present in figure 3.17, there is a good agreement between the values obtained and those theoretically expectable, except for the dimer sample because the purification was not able to effectively separate the dominant fraction of single particles. Despite, it is possible to observe decrease in diffusion coefficient from the stock AuNPs to those functionalized with DNA strands. This corresponds to the expectable result, because of the extra length added by the DNA chains (approx. 8.5 nm) to the particles radius (40 nm). That same expected decrease of diffusion coefficient was not obtained between the functionalized and dimerized structures. This is probably caused by the poor purification that resulted in a ratio between the dimerized and single particles of almost 1:1 in sample A2-b2 (see table 3.3). Another aspect is that, the hydrodynamic radius of dimers is not exactly the double of single AuNPs, being more similar to a rod shape. An equivalent hydrodynamic radius was calculated for a rod object with the diameter of a single particle and an aspect ratio of approx. 2. The values of estimated hydrodynamic radius that were obtained are 40nm, 50nm and 77.6 nm, respectively: for a naked single AuNP; a functionalized AuNP with a 15bp DNA chain; and a dimer of AuNPs[49]. Since the difference in the estimated diffusion coefficient for functionalized or dimerized AuNPs is of only 1,7µm^2/s, it may not be possible to detect it experimentally due to the associated error. Also, the background noise of the measurements performed, suggested sample contamination with fluorescent materials, contamination which could have occurred throughout all the dimer synthesis procedure. All these factors could have prevented the technique to be sensitive enough to detect these subtle variations in diffusion coefficient.

3.1.4 Further attempts at AuNPs dimerization

Due to the low yield of dimers produced, there was not enough quantity of these structures to perform the fluorescence enhancement assays. For that reason, other attempts of particle dimerization were made. Using the same protocol as before, samples were produced with the intent of analysing the ability to form dimers using 20, 40 and 80 nm diameter AuNPs functionalized with PAF30 and SAF30 DNA strands. The conditions for this reaction were as described in 2.4. The salt concentration was decreased due to the severe particle aggregation upon the first addition of citrate buffer with salt, as evident by the immediate loss of the sample's coloration. Nevertheless, some trials of sample preparation were stable enough to allow for electrophoretic separation (figure 3.18).

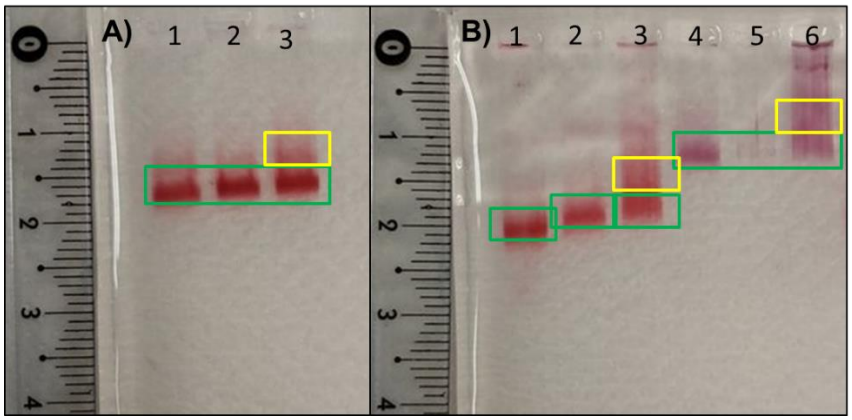

Figure 3.18 – Results of electrophoretic separation. A) Results for 20nm diameter AuNPs, functionalized with PAF30, SAF30 and dimerized in wells 1,2 and 3 respectively. B) Results for 40nm diameter AuNPs, functionalized with PAF30, SAF30 and dimerized in wells 1,2 and 3 respectively and for 80nm diameter AuNPs, functionalized with PAF30, SAF30 and dimerized in wells 1,2 and 3 respectively. The green rectangles identify the first bands removed from the gel for each sample (known as band 1) and the yellow ones the second bands removed (known as band 2).

Some conclusions can be taken from the figure 3.18. Firstly, the distance travelled by the 20nm diameter AuNPs is roughly the same, if not slightly inferior to the one relative to the 40nm AuNPs. This was not supposed to happen, seen as the lighter and smaller particles should flow through the agarose gel with more ease, this consequently suggests that some agglomeration is occurring during the functionalization of the AuNPs with both DNA strands, or that, due to the different DNA coverage between both AuNP sizes, the surface charges differ and therefore the migration speed could differ as well. Also, no bands indicating the presence of dimers are observed, however a trail is observable in the wells containing dimerized samples. This can be due to the hybridization of some complementary DNA strands which result in dimers and other larger aggregates of various sizes and weights or to the incomplete functionalization of AuNPs, which then possess a lesser negative charge and therefore migrate at different rates. It is worthy to note as well that in the functionalized-only 40nm AuNPs, the bands did not migrate the same distance, possibly due to some agglomeration on the SAF30 functionalized sample.

To further assess the type of structures present in the removed bands, an FCS measure was performed to assess their diffusion coefficients, similar to what was done in 3.1.3. The results are displayed in figure 3.19.

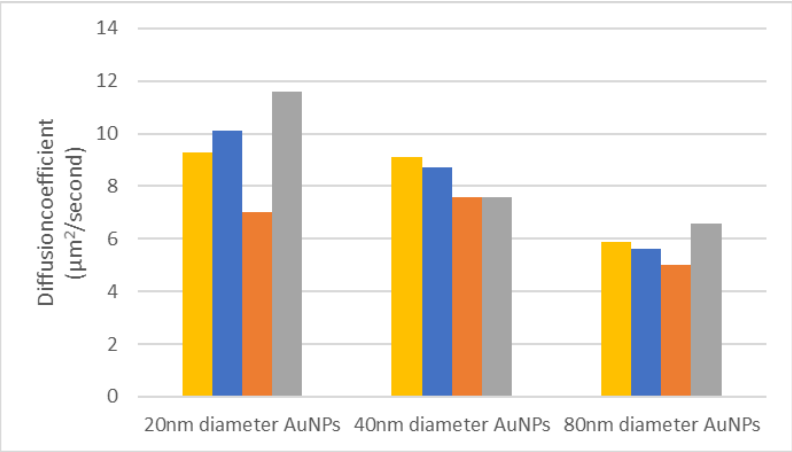

Figure 3.19 - Diffusion coefficients obtained for 20, 40 and 80nm diameter AuNPs. For PAF30 functionalized (yellow), SAF30 functionalized (blue), dimerized (orange) and stock AuNPs (grey).

These results corroborate those observed in the electrophoresis gel, being that there is not a significant difference between the 20 and 40nm diameter AuNPs diffusion coefficient, being concordant with the hypothesis of sample aggregation. Furthermore, a strange result is observed between the dimerized and stock 40 nm AuNPs, as they present the same value for the diffusion coefficient, this is probably due to some error that occurred during the measurements, or some population of agglomerated stock AuNPs that passed through the observational volume very slowly, diminishing the diffusion coefficient measured. To test these hypothesis, TEM images could be obtained and thus revealing the status of the AuNPs present in the different samples. Other approach would be to obtain spectra of these samples and look for any sign of agglomeration or measuring a different stock solution than the one used here, to establish if this diffusion coefficient for the stock AuNPs is correct.

Regardless, it is possible to see a trend of diminishing diffusion coefficient with the increase of AuNP size and the difference between stock and functionalized nanoparticles, hinting that functionalization of the AuNPs' surface is occurring.

3.2 DNA Coverage of AuNPs

Since the formation of dimers in these experiments was subpar to the expectations, it was hypothesised that the DNA strands might have not been covering the NPs efficiently. To test this hypothesis, the number of DNA strands per NP was assessed by fluorescence spectroscopy using fluorescein-labelled oligonucleotides and the values retrieved were compared to the maximum values reported in the literature[38].

To determine the concentration of AuNPs in each sample, their extinction spectrum was measured as mentioned in 2.3, and the respective sample concentration was determined according to the specification sheets from the supplier.

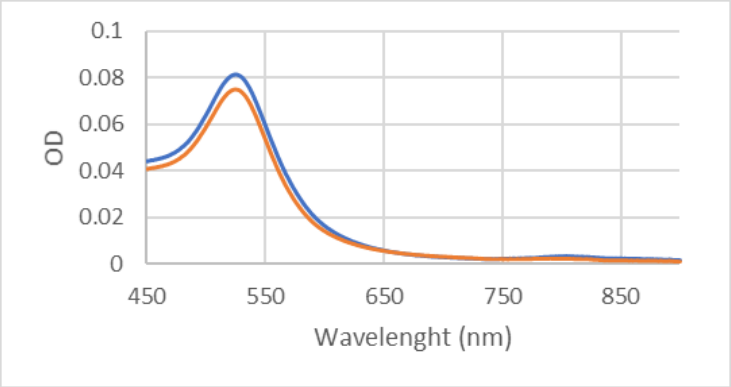

Figure 3. 20 - 20nm functionalized AuNPs' extinction spectrum, with PAF30 (blue) and SAF30 (orange).

There is no significant different in the plasmon peak position for samples of AuNPs functionalized with PAF30 and SAF30, but there is a small difference in the absorbance maximum that is probably due to some loss of material during the functionalization process (figure 3.20).

After washing the functionalized AuNPs to remove all unreacted DNA chains, then the attached DNA chains on the particles were released to be quantified by fluorescence spectroscopy. For this purpose, the functionalized particles were incubated with mercaptoethanol, whose function is to replace the thiolated DNA strands on the NPs' surface[43], and then the emission spectrum of the supernatant of these samples was measured. The integrated area of the emission spectrum was compared to a linear correlation previously established between concentration of dye-labelled DNA and its emission spectra area, in order to assess the concentration extracted from the AuNPs' sample. Note that some assumptions are necessary for this to apply: it is assumed that each strand of DNA contains one molecule of the fluorophore, that the entirety of DNA strands was removed from the NPs by the mercaptoethanol and also, that no free DNA strands are present in the sample previous to the mercaptoethanol treatment. Finally, by dividing the dye-labelled DNA concentration by the NPs concentration, we obtain the number of DNA strands per NP (table 3.4).

Table 3.4 - Results for the DNA coverage of various size NPs.

NP size(nm)	DNA Strand	Expected ratio of DNA strands per NP[38]	Obtained ratio of DNA strands per NP
20nm	PAF30	180	142
	SAF30		142
40nm	PAF30	430	453
	SAF30		543
80nm	PAF30	1400	1408
	SAF30		1310

As presented in the table 3.4, the difference between the expected ratio, based on literature, and the experimentally obtained results do not differ significantly. And those differences can be due to the error inherent to the experiment setup, or even to the fact of, as shown in figure 3.16, the nanoparticles are not perfect spheres and may vary slightly in size, which could lead to the discrepancy observed between expected and actual results.

So, it is possible to conclude that the difficulty in obtaining nanoparticle dimers is probably not due to the lack of coverage of DNA strands in the NPs.

Another interesting result observed in this experiment, it is the quenching effect of the nanoparticles have on the fluorescence of fluorescein dye. By comparing the emission spectra of the sample with the DNA strand attached to the NPs and the sample with just the DNA strands (after removal with mercaptoethanol), it is possible to see a significant change in the amount of fluorescence of both samples, as shown in the figure below.

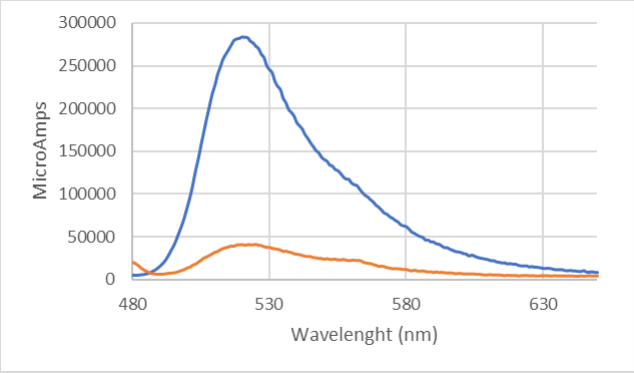

Figure 3.21 - Comparison of emission spectra of PAF30 functionalized 20nm diameter AuNPs (orange) and for the supernatant collected after mercaptoethanol (blue) obtained for an excitation wavelength of 470nm.

As seen in figure 3.21, the difference between the fluorescence in the presence or absence of NPs is clear. This is most likely due to a quenching effect of the NPs, since the amount of fluorescein to be measured is equal in both samples, if not, slightly lower in the case of the supernatant due to the lack of complete efficiency in the removal of the DNA strands from the NPs. This finding is supported by literature which already showed this phenomenon to occur[50]-[53]. This happens because the fluorophore's quantum yield is decreased by loss of energy to the metallic structure which is not compensated by the increase of excitation and radiative rates from the enhanced electric field of the surface plasmon.

Table 3.5 – I/I_0 values for BF1-BT molecules attached to different size AuNPs.

Sample	I/I_0 (%)
PAF30 - 20nm AuNPs	17,4
SAF30 - 20nm AuNPs	17,9
PAF30 - 40nm AuNPs	20,6
SAF30 - 40nm AuNPs	18,8
PAF30 - 80nm AuNPs	70,1
SAF30 - 80nm AuNPs	56,1

Moreover, since various sizes of nanoparticles were tested it is also possible to establish a correlation between the nanoparticle size and its quenching effectiveness. As seen in table 3.5, the smaller the metallic nanostructure, the higher the quenching effect. This result is also in accordance with the literature[53].

3.3 Fluorescence enhancement by Single AuNRs

In order to assess the enhancing capabilities of plasmonic structures, an experiment was designed to discover the potential of fluorescence enhancement for AlPcTS and the DNA spacer BF1-BT with the fluorophore ATTO-647N. Due to the problems felt with the production of dimers, either be it due to lack of efficacy or to lack of reproductivity of the results obtained in the first experiments performed, it was decided to perform this fluorescence enhancing experiments using gold nanorods. Due to their shape, the enhancement factors obtained are expected to be higher than if single nanoparticles were used, making them a closer approximation to the effects of using dimerized structures[54], bellow is an image of a NR and the calculated hotspots for fluorescence enhancement.

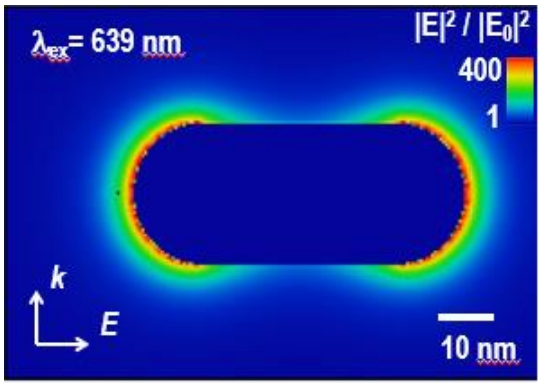

Figure 3.22 - Calculated near-field intensity map of a gold nanorod[55].

3.3.1 Fluorescence enhancement of AlPcTS by Single AuNRs

The surface immobilized NRs were detected using their photoluminescence emission in CFM images using as excitation source the 639 nm laser. This allowed us to localize NRs present on the glass surface (figure 3.23).

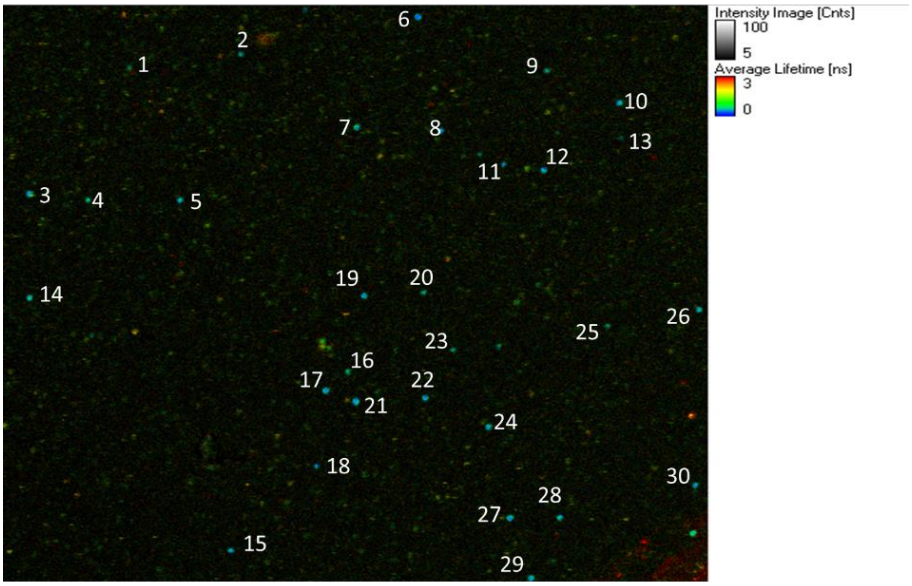

Figure 3.23 - CFM image of a glass slide with AUT functionalized NRs. Image obtained in PBS with dimensions of 80x80µm, with the laser of 639nm with a 0.024µm/pixel resolution.

The NRs should have a photoluminescence spectrum with a longitudinal plasmon resonance band overlapping the absorption and emission spectra of the fluorophore used, in order to enhance its fluorescent capabilities[56]-[58]. Furthermore, it is reported that the maximum enhancement of fluorescence of a molecule with a metallic structure, occurs when its peak of emission is slightly shifted toward lower energy (longer wavelength) than the peak for the surface plasmon band. However, it is still required an overlap between the LSPR band and the fluorophore's emission spectra[56][57] (see figure 3.24).

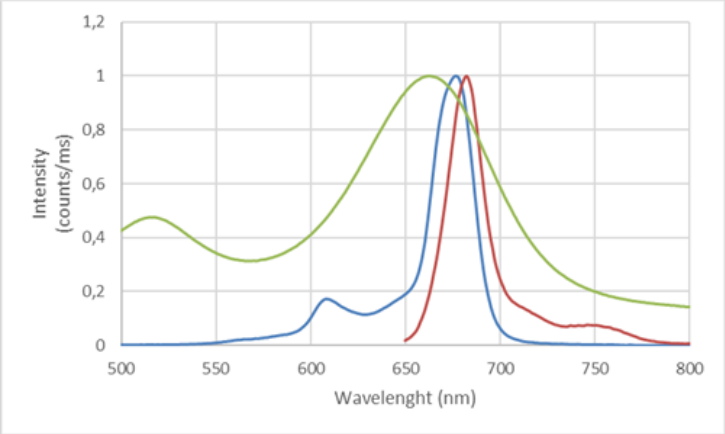

Figure 3.24 – Absorbance (blue) and emission (red) spectra of AlPcTS overlapping with the extinction spectrum of stock nanorods (green).

As mentioned previously, the NRs were coated with AUT monolayer. This allows to create a spacing layer between the NR and the fluorescent molecule, in order to avoid quenching effects that dominate the antenna performance close the metal surface. The coating of the NRs was confirmed to be successful from monitoring the red-shift of the plasmon peak in the single-particle emission spectrum of a selected set of particles[59].

Before the enhancement experiment, control measurements were performed to characterize the emission signal from the nanoparticles alone. These measurements were performed by focusing the laser in the centre of each particle's emission spot (or psf) and acquiring a time trace for 30 seconds at an excitation energy of 0,4kW/cm^2. These measures allow to check the background signal in the absence of the fluorophore, which will be later compared with measurements taken in the presence of AlPcTS. Ideally, the time trace should be constant and without any bursts of intensity, since these can only happen if impurities are present in the sample and eventually cross the NRs hotspot. An example of such measurement belonging to particle 1 is present in figure 3.25.

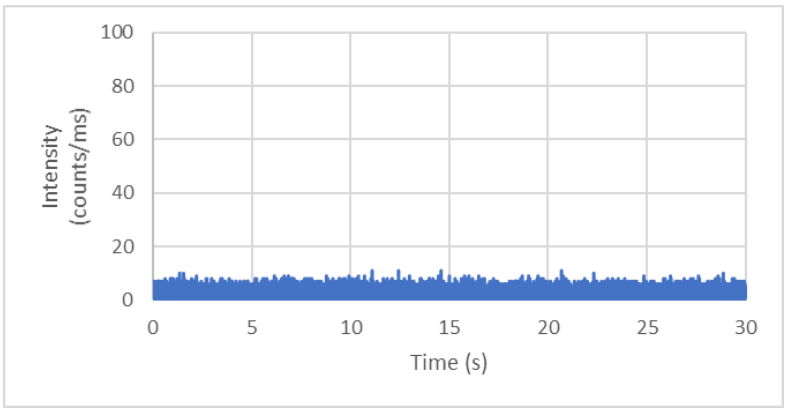

Figure 3.25 – Intensity time trace of AuNR designated as 1 in figure 3.13.

The AlPcTS was then added to a final concentration of 10nM and the fluorescence intensity of each nanorod was measured again during a time trace acquisition. For this purpose, the laser was focused on the nanorod's emission spot (or psf) and the intensity fluctuations were measured for 60 seconds. The reasoning being that, the fluorescent molecules are able to diffuse freely through the solution and each time that one crosses the plasmonic hotspot at the NRs' tips, a burst of fluorescence intensity will be observed, as represented in figure 3.26.

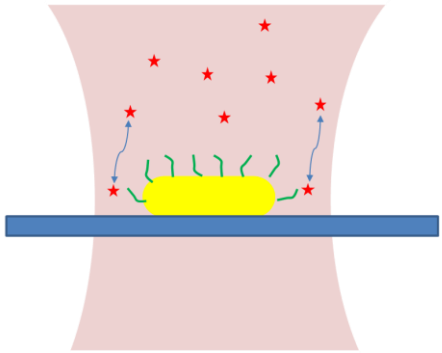

Figure 3.26 – Schematic representation of the intensification phenomenon produced by the AUT functionalized NRs. The AlPcTS molecules (★) are able to freely diffuse through the solution.

In order to be able to calculate the fluorescence enhancement of the NRs on the fluorophore molecules, the non-enhanced intensity of AlPcTS must be known. In this case, that value had already been calculated through previous experiments performed in the group, as described in 2.6.1. The value obtained was 0,24 counts-per-molecule/ms with a standard deviation of 0,11.

The intensity time traces of NRs with AlPcTS in solution show a background signal, corresponding to the NRs' emission, and occasionally strong emission bursts, which are assumed to correspond to the passage of one AlPcTS molecule through the NRs' hotspot. This is not always the case, since some fluorescent molecules can interact with the AUT coating layer, or the glass surface, and reside in the enhancement hotspot longer, thus, producing long events of enhanced emission. In other cases, there were no significant bursts detected, indicating that no molecules interacted with the NRs' hotspot during the measurement, probably because, despite the AuNR being visible in the CFM images, their hotspots

might be blocked by something present in the surface obstructing physically or due to repulsion of charges. An example of a trace with individual bursts and some selected events of enhanced emission bursts are presented in figure 3.27.

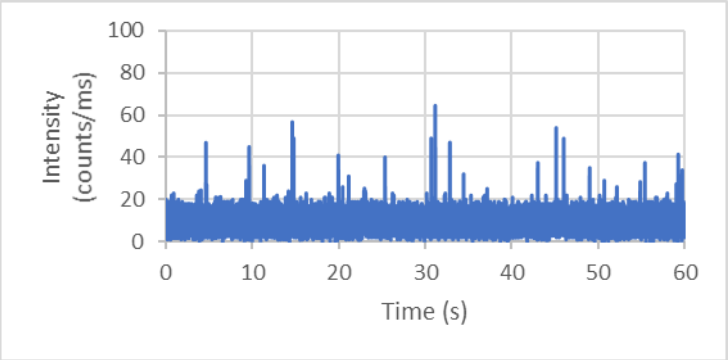

Figure 3.27 – Intensity variation of a AuNR (identified as 1 in figure 3.13) in the presence of BF1-BT.

It is possible to see a clear difference between the MCS trace of AuNRs in absence or presence of a fluorophore. It can be concluded then, that these bursts are due to the presence of AlPcTS in the enhancement hotspots for the AuNR located in the observational volume.

The intensity time traces showing clear enhanced emission bursts were then analysed according to the "cherry-picking" method, described in 2.6.3, in order to obtain the maximum enhancement factors relative to each measurement. Also, the FOM_{enh} values were obtained by multiplying the enhancement factor by the quantum yield of the fluorophore used, which in this case is 34%[60].

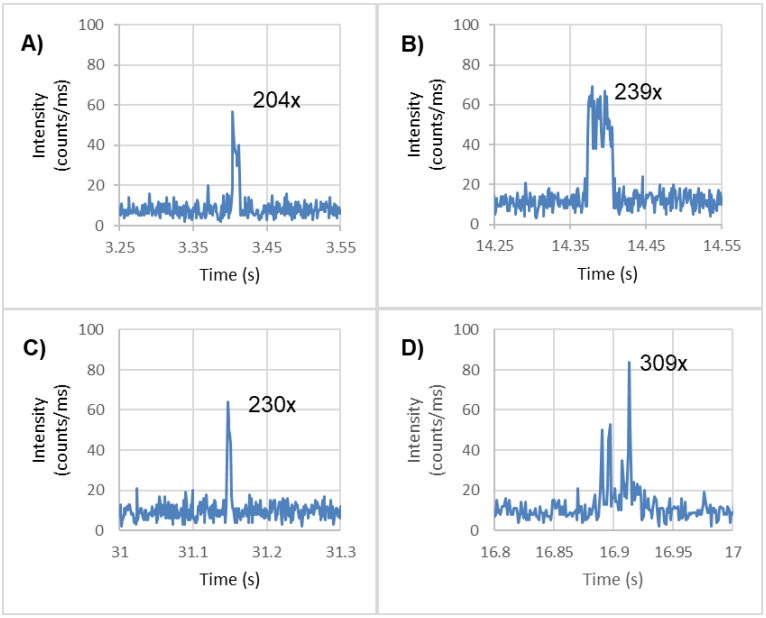

Figure 3.28 – Examples for detected maximum intensity bursts for the nanoparticles identified in figure 3.22, AuNRs 1, 22, 25 and 30 for A), B), C) and D) respectively.

Table 3.6 - Number of events, enhancement factors and figures of merit for the different nanorods measured.

AuNR	Number of events	ξMax (with SD)	FOM_{enh}
1	23	204 ± 98	69
3	22	145 ± 73	49
4	132	175 ± 86	60
5	29	139 ± 70	47
7	57	320 ± 151	109
9	50	220 ± 105	75
10	42	219 ± 106	75
11	10	154 ± 76	52
12	79	221 ± 107	75
17	22	160 ± 80	55
18	42	169 ± 83	57
20	28	149 ± 74	51
22	20	239 ± 115	81
24	72	167 ± 83	57
25	35	230 ± 110	78
26	32	172 ± 85	58
27	18	169 ± 84	58
29	36	219 ± 106	75
30	54	309 ± 146	105
Average	42	199 ± 97	68

These results present in table 3.6, demonstrate the enhancement potential of a gold NR antenna on the fluorescence of AlPcTS, which is about two orders of magnitude increase in the detected emission when compared to the same molecule alone.

In this experiment, the emission spectra for these AuNRs was not collected and so it is not possible to make any analysis of the effect of the longitudinal peak's wavelength and the enhancement factor. Nonetheless, the AuNRs chosen present a very similar intensity and size as observed in the CFM image to those previously observed in other surface areas where immobilized single gold NRs were found, as confirmed from their single-particle emission spectra.

3.3.2 Fluorescence enhancement of BF1-BT by Single AuNRs

The experiment described here is similar to that used in the previous section, but the fluorescent molecule was changed from AlPcTS to a thiolated DNA spacer BF1-BT that is 10-bp long and is labelled with Atto-647N dye.

After the AuNR deposition on a silanized glass slide, a CFM image was taken to localize the nanorods on the surface. The emission spectrum of the individual AuNRs was measured using the 482nm laser as excitation source.

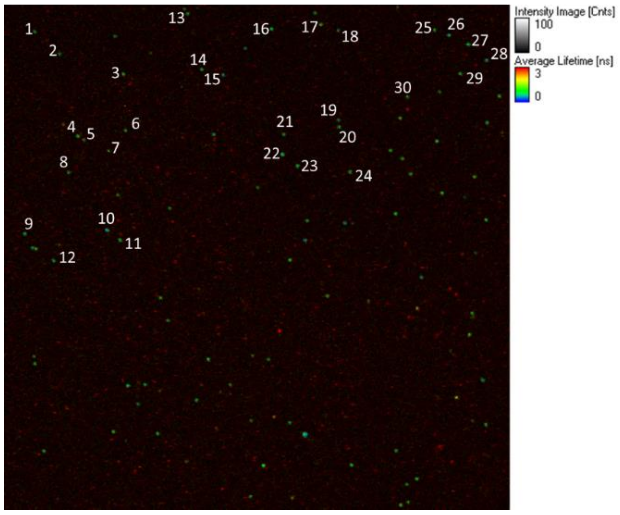

Figure 3.29 - CFM image of a glass slide with deposited AuNRs. Image obtained in PBS with dimensions of 80x80µm, with the laser of 482nm with a 0.024µm/pixel resolution.

The emission spectra allow to confirm that indeed single AuNPs are being measured, and not particle aggregates. Furthermore, it was also confirmed the overlap between the longitudinal surface plasmon band and the absorbance or emission spectra of the fluorophore, which as previously described (3.3) is crucial for fluorescence enhancement to occur.

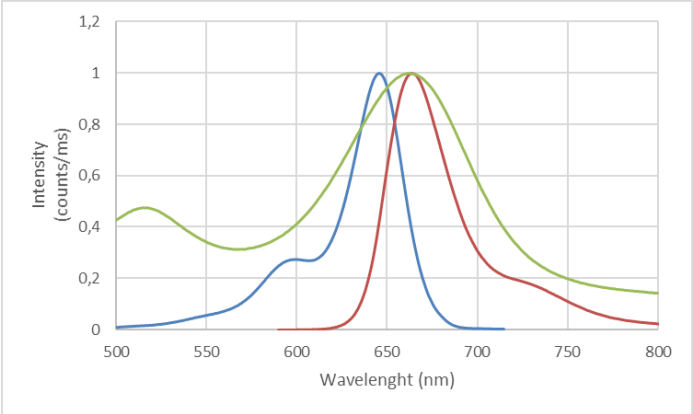

Figure 3.30 – Absorbance (blue) and emission (red) spectra of ATTO-647N overlapping with the extinction spectrum of stock nanorods (green) [61].

For this experiment, the AuNRs selected are labelled 4, 9, 25, 26 and 27 in figure 3.28. Some of the spectra obtained for the AuNRs, are shown in figure 3.31, corresponding to two particles from the selected ones that were studied throughout this experiment.

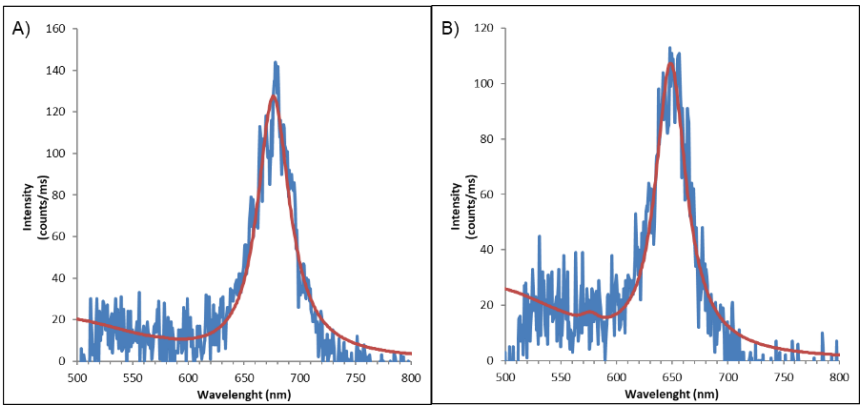

Figure 3.31 - Emission spectra of AuNRs obtained with the spectrometer coupled to the CFM, excited with the 482nm laser. The experimental spectra are represented in blue, and fitted lorentzian curves are shown in red.

The spectra of selected particles are very similar in shape with a peak being observed at around 650-700nm, corresponding to the longitudinal plasmon of the nanorod. The transversal plasmon that normally appears in the 500-550 nm wavelength range was not observed clearly, since the filter used in the CFM only allows for wavelengths above 510nm to pass. Another issue is light scattering from the laser or luminescence from the optics used, that overlap with the spectral region where the first peak should be observed. As expected, the peak position of the longitudinal surface plasmon changes from particle to particle due to sample heterogeneity in particle size or shape, because this plasmon resonance changes sensibly with the aspect ratio of the nanorods. This will affect the overlap between the plasmon and the absorption/emission spectra of the fluorophore, which should affect the magnitude of the enhancement effect. In this regard, it is even more crucial the overlap of the plasmon peak with the excitation laser wavelength used for the enhancement experiment.

For this purpose, it was used an excitation laser at 639nm. Firstly, a CFM image was acquired to confirm that the same position on the surface was maintained when the laser was changed. Before the addition of the fluorophore, the intensity time traces on the selected AuNRs were measured to serve as a control in order to check that no bursts of fluorescence are obtained when no fluorophore is present. An example of one of these time traces is presented in figure 3.32.

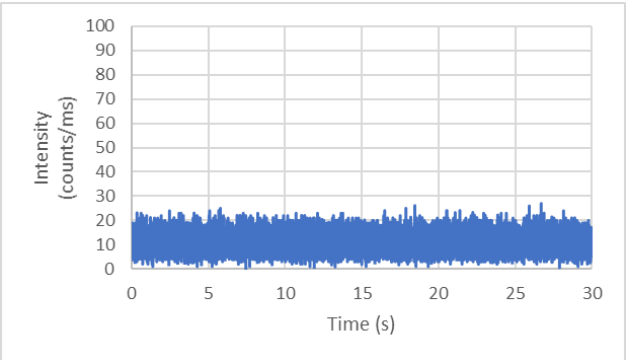

Figure 3.32 – Intensity time trace of AuNR designated as 25 in figure 3.28.

The next step was the addition of the BF1-BT hybrid, as described in 2.7.2. The aim of this experiment was to test the enhancement factors produced by the AuNRs on the fluorophore chosen for the molecular beacon BF1-BD2. Therefore, instead of using the full structure of the molecular beacon, it

was employed a shorter version containing only the ds-DNA spacer and the fluorophore, but not the DNA hairpin nor the quencher that are present only in the BF1-BD2 hybrid.

The intensity time traces of the BF1-BT hybrid interacting with surface-immobilized AuNRs were measured using an excitation energy of 1,71kW/cm^2. Following the same procedure as described in 3.3, the nanorods which showed the most intense fluorescence bursts were selected to be further analysed. This analysis was performed using the two methods described in 2.7.2, in order to compare these methods' influence in the final results.

In order to calculate enhancement factors, the brightness of an individual fluorophore molecule must be known, which in this case is 2,46 counts/ms, at an excitation energy of 1,71kW/cm^2.

3.3.2.1 Analysis by "cherry-picking"

This analysis was performed similarly to the one shown in 3.3. The complete time trace of particle 25 and the most intense bursts extracted from the time traces of selected AuNRs, are presented in figure 3.33.

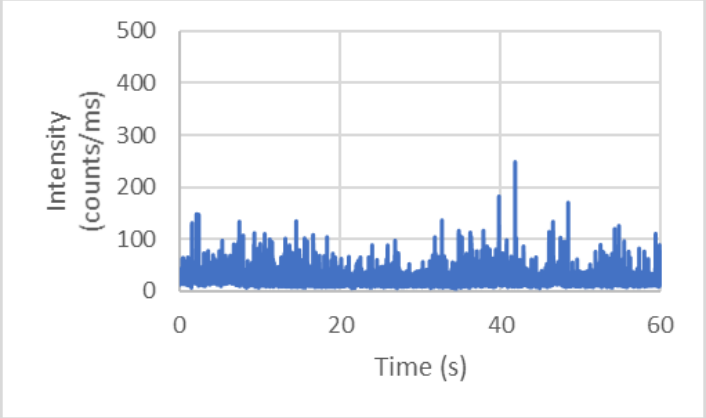

Figure 3.33 - Intensity time trace of AuNR identified as 25 in figure 3.28 in the presence of BF1-BT hybrid.

It is possible to observe a clear difference between the time traces of AuNR labelled as 25 in the absence and presence of the fluorophore. This shows that the bursts obtained are due to the presence of BF1-BT hybrids interacting with the plasmonic hot-spots produced by the AuNR.

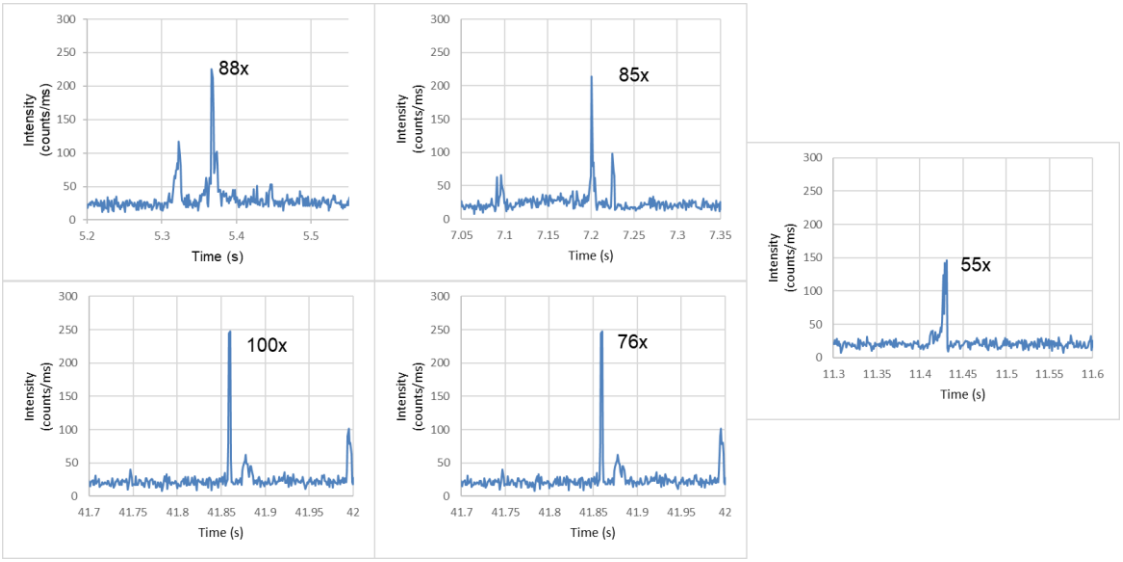

Figure 3.34 - Maximum intensity bursts detected for the nanoparticles identified in figure 3.28 with the labels 4, 9, 25, 26 and 27 that correspond to traces A), B), C), D) and E), respectively. The number inside each graph indicates the respective enhancement factors.

The enhancement factors were calculated from the maximum intensity of the strongest burst subtracted from the background intensity for the AuNRs and divided by the individual brightness of a fluorophore molecule. Subsequently, the values of the figure-of-merit (FOM_{enh}) were obtained by multiplying the enhancement factors by the quantum-yield of the fluorophore. The results obtained are shown in table 3.7.

Table 3.7 - Number of events, position of the LSPR, enhancement factors and figures of merit for the different nanorods measured (with correspondent standard deviations (SD)), relative to the "cherry-picking" analysis method of the enhancement experiments performed with BF1-BT and AuNRS.

AuNR	Number of events	LSPR position (nm)	ξMax (with SD)	FOM_{enh}
4	255	676	88 ± 11	57
9	174	662	85 ± 10	55
25	356	685	100 ± 12	65
26	253	649	76 ± 10	50
27	229	679	55 ± 8	36
Average	253	670	81 ± 10	53

The enhancement factors of the different AuNRs were plotted against the position of their longitudinal plasmon determined from the single-particle emission spectra (figure 3.35). In the same plot, the experimental enhancement factor are compared to theoretical values that had been previously calculated, via discrete dipole approximation, by the research group that hosted this project[61].

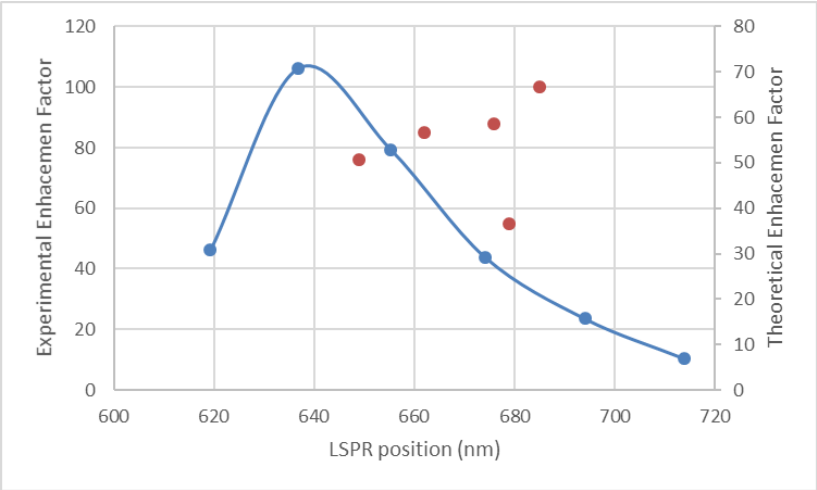

Figure 3.35 – Correlation of the top enhancement factors obtained experimentally with the "cherry-picking" analysis method (red) and theoretically (blue), for the BF1-BT fluorescence enhancement assay with AuNRs.

By comparing the experimental and theoretical values, it is observable that they are within the same order of magnitude of the theoretical ones, although not exactly coincident. Surprisingly, the experimental factors are slightly larger than those estimated from the simulation, which can be due to experimental bias. Since the AuNRs chosen to be studied, are the ones that present the highest fluorescence intensities, this tips the values toward higher enhancement factors, however the theoretical values, are calculated for the optimum enhancement of fluorescence, so despite this they should be higher.

Other explanation might be that the maximum values obtained through this analysis method are not representative of the real events, as more than one molecule of fluorophore might be present in the hotspot at the same time, thus having their intensities added and appearing as one burst only.

Also, the experimental factors do not follow the predicted trend with the longitudinal plasmon resonance wavelength, because experimental values seem to be scattered.

3.3.2.2 Analysis by extrapolation

This analysis, as described in 2.6.4, estimates the maximum intensity of bursts produced by performing a tail fit to the intensity frequency histogram produced by the FCS measurements. Examples of these histograms before and after the addition of BF1-BT hybrid are given in figure 3.36.

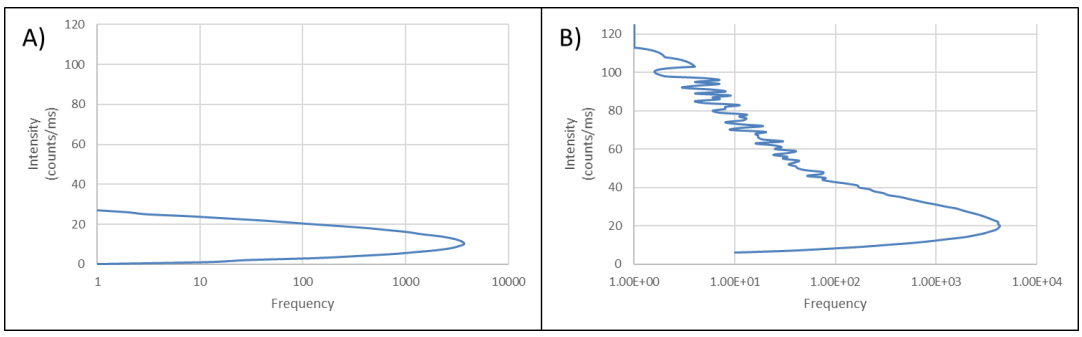

Figure 3.36 – Intensity frequency histogram for AuNR 25 before (A) and after the addition (B) of BF1-BT.

A clear difference is observed between the two histograms above. In the absence of BF1-BT, the bursts of intensity are not present. Therefore, the background signal results in an intensity histogram with a gaussian shape, from which the mean background level due to the AuNR emission can be obtained. The multiple events of strong emission due to the presence of a BF1-BT molecule in the observation volume changes the intensity histogram by adding an exponential tail on the side of large count rates. The maximum intensity can be estimated from a tail fit of the histogram shown in image B. An example of the curve fitting performed using a gaussian curve to fit the background intensity and a tail to determine the maximum burst intensity is shown in figure 3.37.

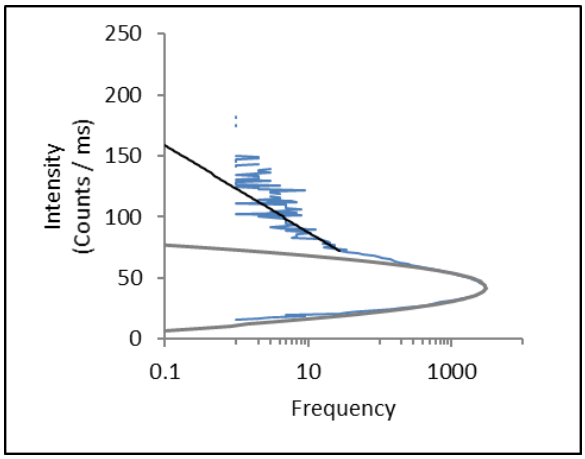

Figure 3.37 – Extrapolation of the maximum burst intensity by performing a tail fit (black) to the intensity frequency histogram for AuNR number 25 in the presence of BF1-BT hybrid. A gaussian curve is also adjusted to obtain the background intensity from emission of the AuNR (grey).

From this analysis, the values for enhancement factors were re-calculated (table 3.8).

Table 3.8 - Number of events, position of the LSPR, enhancement factors and figures of merit for the selected nanorods (with correspondent standard deviations, SD), obtained by the extrapolation analysis method for emission enhancement of BF1-BT fluorescence by AuNRs.

AuNR	Number of events	LSPR position (nm)	ξMax (with SD)	FOM_{enh}
4	255	676	78 ± 6	50
9	174	662	38 ± 4	25
25	356	685	70 ± 5	45
26	253	649	59 ± 5	38
27	229	679	34 ± 5	22
Average	253	670	56 ± 5	36

A correlation between the position of the AuNR LSPR and the enhancement factor was assessed (Figure 3.38).

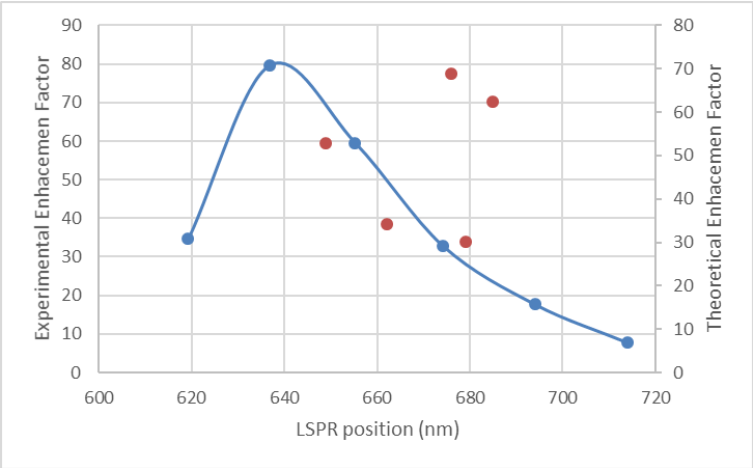

Figure 3.38 – Correlation of the top enhancement factors obtained experimentally with the extrapolation analysis method (red) and theoretically (blue), for the BF1-BT fluorescence enhancement assay with AuNRs.

As it was the case in the same correlation performed with the “cherry-picking” method, the experimental data matches the order of magnitude theoretically calculated for the enhancement factors. Even though scattering of experimental values is also observed here, a better comparison is obtained mainly due to the lower experimental enhancement factors determined by this analysis method.

3.3.2.3 Comparison of analysis methods

Even though, as described in the literature[54], both methods provide similar results overall. However, some of the points vary drastically according to the analysis method used. This is observable in AuNR no. 9, which gives an enhancement factor of 85 times with the “cherry-picking” method, but only 38 times when the extrapolation method was used. This happens because the maximum burst of intensity observed in the time traces was much higher than any other point measured. So, the importance of that event, which could be an anomaly, is overestimated by “cherry-picking” method. On the other hand, when using the extrapolation method, the contribution of all the other bursts correspond to a more comprehensive sampling and the importance of that point gets diluted.

Therefore, the extrapolation method appears to be more reliable, however, this method may not always be applicable, as mentioned before. So, for those cases, the “cherry-picking” method presents itself as fair alternative, as long as the maximum burst does not deviate significantly from other burst intensities. Furthermore, for both analysis methods, these results are more in accordance with the theoretical values[61].

3.3.2.4 Enhancement factor variation with excitation energy

In order to assess if the maximum intensity of the strongest event would vary linearly with the excitation energy, this experimental parameter was screened and the analysed results for the two methods discussed above are presented in figure 3.39 and 3.40.

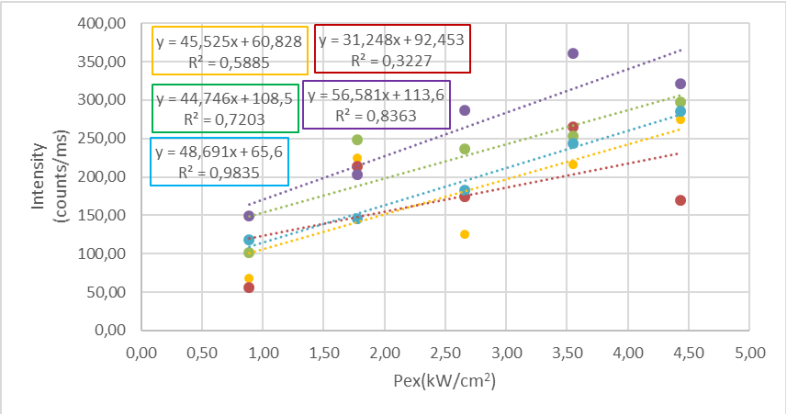

Figure 3.39 – Correlation of the maximum intensity obtained for each AuNR, using the "cherry-picking" analysis method with the variation of excitation energy, the equations and R^2 of the different linear regressions are also presented. AuNR 1 (yellow), AuNR 9 (red), AuNR 25 (green), AuNR 26 (purple) and AuNR 27 (blue).

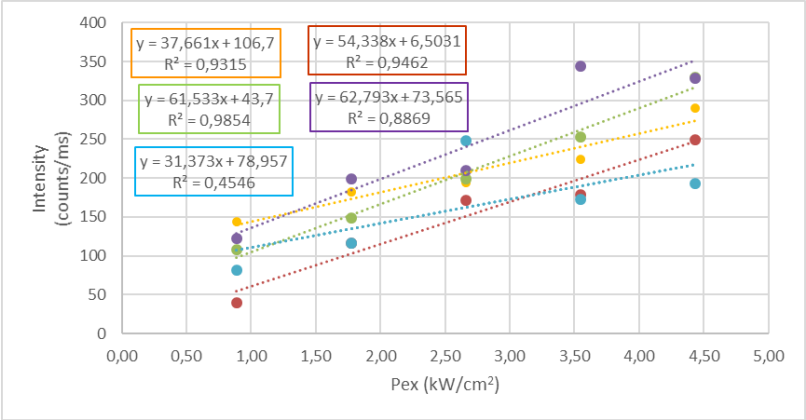

Figure 3.40 – Correlation of the maximum intensity obtained for each AuNR, using the extrapolation analysis method with the variation of excitation energy, the equations and R^2 of the different linear regressions are also presented. AuNR 1 (yellow), AuNR 9 (red), AuNR 25 (green), AuNR 26 (purple) and AuNR 27 (blue).

These results help to corroborate the discussion remarks in 3.3.2.3, since there is a better correlation of the maximum intensity bursts and the variation of excitation energy in the data obtained by the extrapolation method.

Despite that, it is obvious that the correlation is not perfect. This can be due to experimental uncertainty from poor sampling which prevents these methods from assessing correctly the maximum intensities for each excitation energy. Therefore, the data is too disperse to enable any conclusion from being taken.

3.4 2-D organized AuNP film

In order, to achieve a film of closely-packed AuNPs, with high fluorescence enhancing capacities, depositions were performed using the protocol described by Liebig, *et al.* [34], based on the formation of a self-assembled monolayer of AuNPs in the air-liquid interface of a droplet, by formation of AuNP-coated vesicles upon the addition of an ethanol-toluene mixture, and the consequent separation of the different phases.

To understand the morphology of the AuNP layer resultant from this deposition method, various methods were implemented. To begin with, optical microscopy was used, allowing not only to see the structures

in transmission mode, but also the spatial distribution of emission from their CFM images and emission spectra.

3.4.1 Characterization of films from AuNPs of 20nm

The results for the deposition of 20nm AuNPs are presented in figure 3.41.

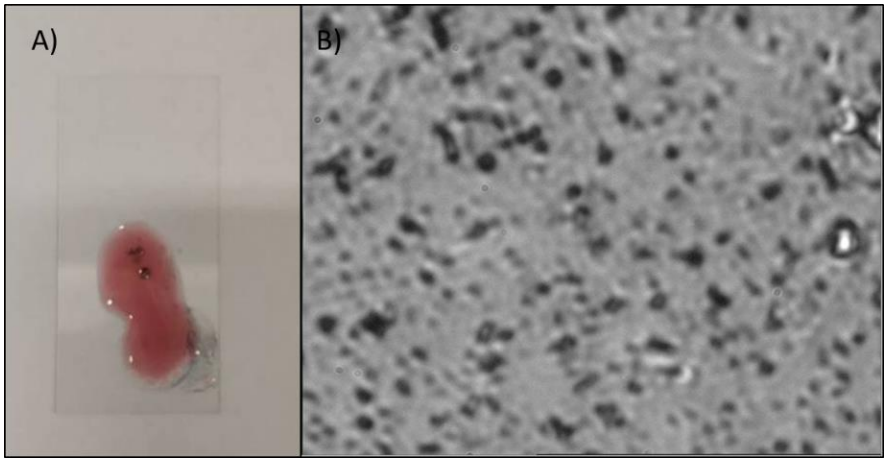

Figure 3.41 – Images of the film deposition of AuNPs sized 20nm. Picture of the glass slide after the addition of the ethanol-toluene mixture to the droplet containing the AuNPs (A) and image of the surface obtained through the optical microscope in transmission mode (B).

In figure 3.41-A, it is possible to see some agglomeration, possibly due to formation of ethanol-toluene mixture vesicles coated with AuNPs, as described in the literature[34]. Nevertheless, it is possible to see the droplet spreading through the glass surface, due to a change in wetting properties caused by the addition of the solvent mixture. Image B was obtained by observing the surface under the optical microscope in transmission mode and selecting an area with high density of these structures. It is possible to distinguish two features, the darker spots, which could be large agglomerates and stacking of AuNPs and the background, which shows a grainy structure probably due to light scattering from isolated AuNPs.

Next a FLIM image was taken of the surface presented in figure 3.41-B and emission spectra of different structures were taken.

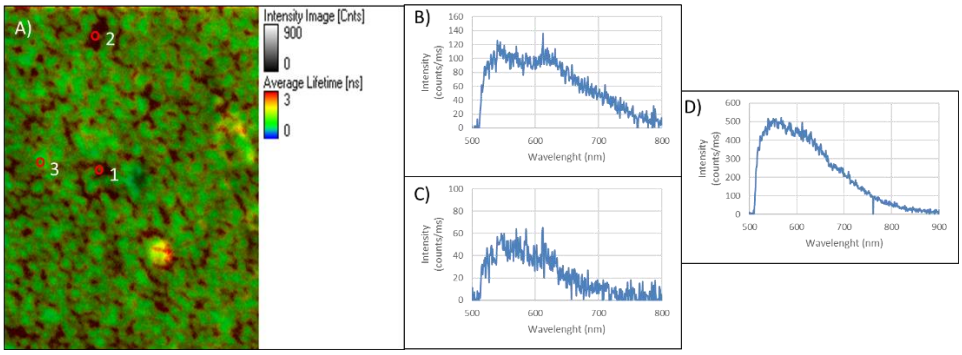

Figure 3.42 – FLIM image of the surface shown in figure 3.41 and emission spectra of the points marked with red circles in image A. The spectra relative to the points 1, 2 and 3 are presented in figures B, C and D respectively.

In the CFM image (figure 3.42) is possible to observe that the darker spots in figure 3.41-B are the brightest. The measured spectra suggest that the fainter signals (1 and 2) in the FLIM image are similar

to dimers of AuNPs or at least closely packed AuNPs. On the other hand, the spectrum of the brightest spot (3) suggests the presence of large agglomerates, which result in a broader spectral lineshape and higher emission intensities.

The same surfaces were also visualized using SEM. Some images illustrative of the structures seen are presented in figure 3.43.

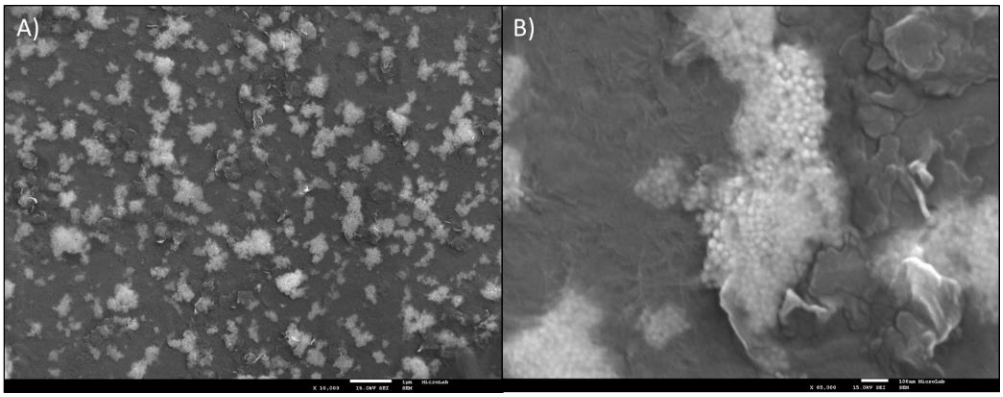

Figure 3.43 – SEM images of the film obtained from deposition of AuNPs sized 20nm. Images with less (A) and more (B) amplification.

In these images the presence of islands of closely-packed AuNPs are clearly visible, thus, confirming the hypothesis suggested from the analysis of the optical microscopy images. However, some substance appears to be covering the AuNPs. The atomic composition of this substance was assessed by making an energy-dispersive X-ray analysis and it was composed of mostly of carbon and nitrogen, so it was likely an organic contamination. This could have occurred during the preparation of the sample or throughout its manipulation.

3.4.2 Characterization of films from AuNPs of 40nm

The results for the films obtained from deposition of AuNPs sized 40 nm are presented in figure 3.44.

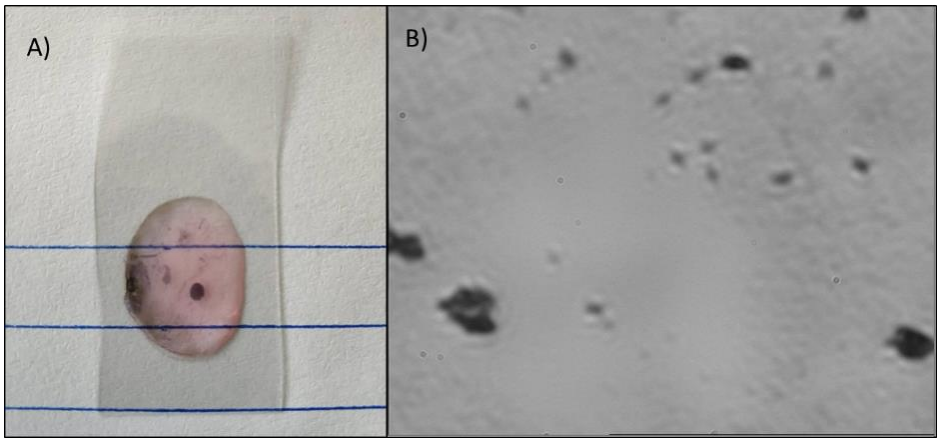

Figure 3.44 – Images of the film deposition of AuNPs sized 40nm. Picture of the glass slide after the addition of the ethanol-toluene mixture to the droplet containing the AuNPs (A) and image of the surface obtained through the optical microscope attached to the CFM (B).

The results are very similar to those reported in 3.4.1. While some larger aggregates are observed in image B of the figure above, it is also possible to see areas that appear to be depleted of AuNPs.

A CFM image of the area relative to image B was taken and some emission spectra were obtained in order to characterise the structures observed.

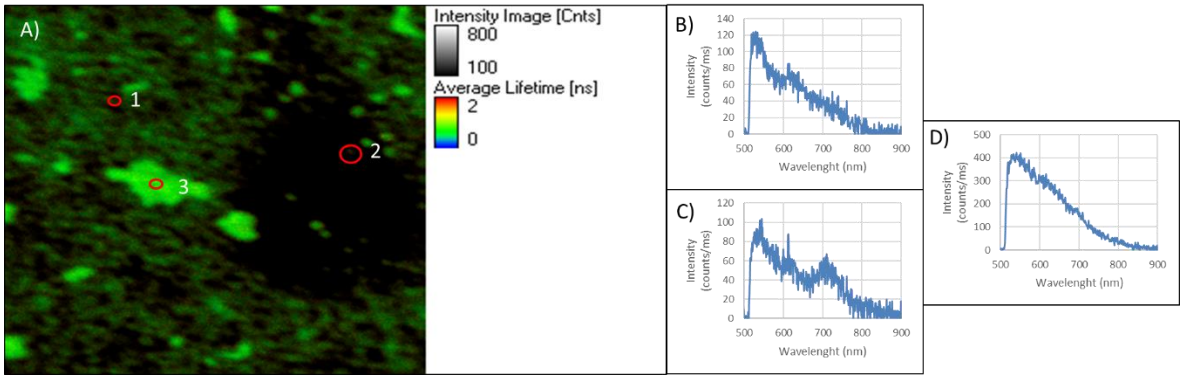

Figure 3.45 – FLIM image of the surface present in figure 3.44 (A) and emission spectra of the points marked with red circles in image A. The spectra relative to the points 1, 2 and 3 are present in figures B, C and D respectively.

The spectra of figure 3.45 suggest that the brightest spots (3) are large agglomerates, as before, these are characterised by a broader and more intense spectrum. As for the less intense spots, they appear to be dimerized AuNPs or very closely packed AuNPs. This is a promising result, since this type of spots is the most abundant in the images observed.

Following this the samples were visualized using SEM.

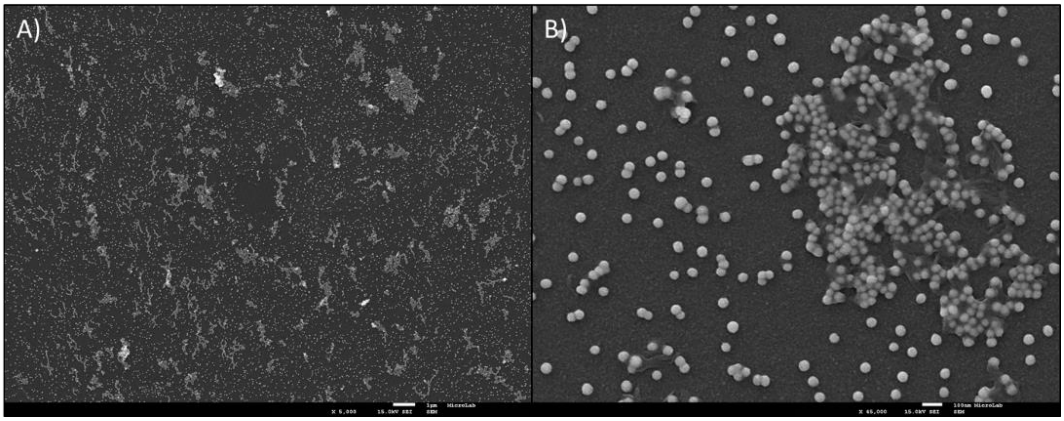

Figure 3.46 – SEM images of the film obtained from deposition of AuNPs sized 40nm. Images with less (A) and more (B) amplification.

The previous observations are confirmed by the images present in figure 3.46, as expected islands of AuNPs are present and rest of the surface is covered either with single, dimerized AuNPs or other larger aggregates.

3.4.3 Characterization of films from AuNPs of 80nm

The results for the films obtained from deposition of AuNPs sized 80 nm are presented in figure 3.47.

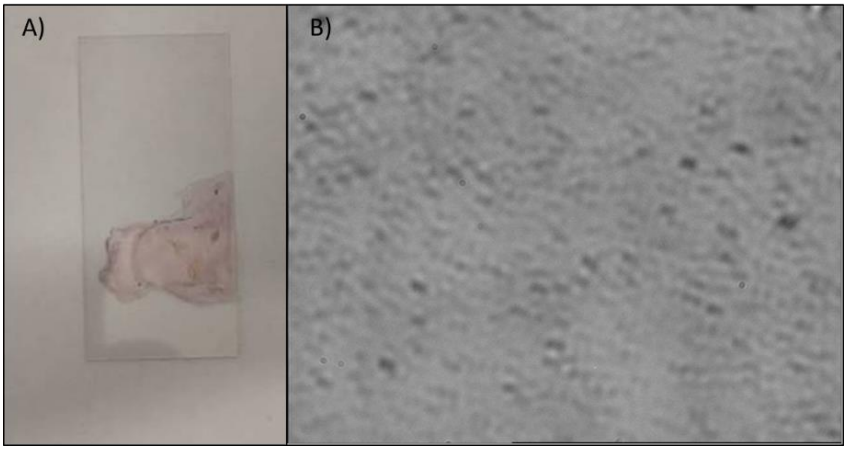

Figure 3.47 – Images of the film deposition of AuNPs sized 80nm. Picture of the glass slide after the addition of the ethanol-toluene mixture to the droplet containing the AuNPs (A) and image of the surface obtained through the optical microscope attached to the CFM (B).

The results are very similar to the ones obtained for the previous depositions with other AuNP sizes. However, in the image B) of the figure above, the particle distribution observed seems to be more homogeneous without large AuNPs islands.

A FLIM image of that area was then taken and some emission spectra obtained in order to characterise the structures observed.

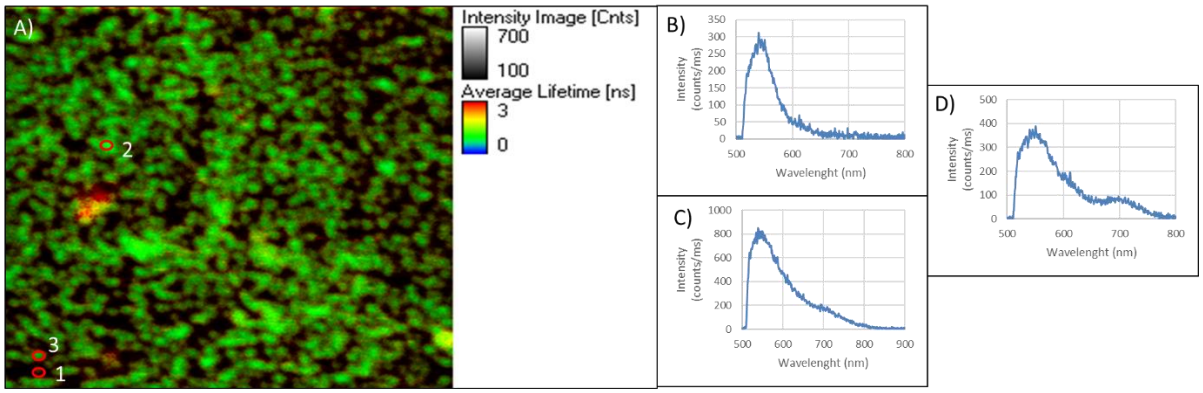

Figure 3.48 – FLIM image of the surface present in figure 3.47 (A) and emission spectra of the points marked with red circles in image A. The spectra relative to the points 1, 2 and 3 are present in figures B, C and D respectively.

In this surface, the fainter points seem to be of single AuNPs (B), while the more intense have spectra similar to those of dimers or closely enough packed AuNPs (C and D).

SEM images were taken to verify the real morphology of the structures observed.

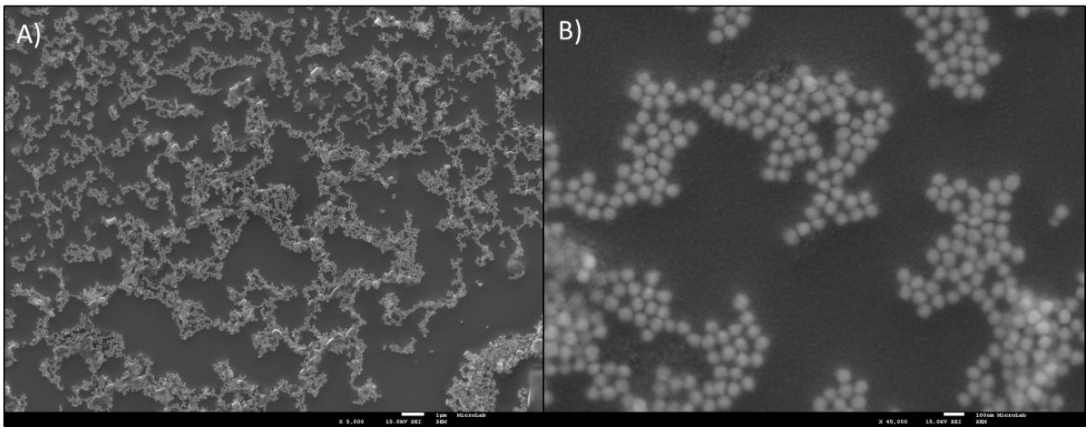

Figure 3.49 – SEM images of the film obtained from deposition of AuNPs sized 80nm. Images with less (A) and more (B) amplification.

In the images obtained through Sem (see figure 3.49), islands of AuNPs which were not detected previously are present, despite that a good distribution is observed in both the more and less amplified image, showing evidence of closely packed AuNPs as intended. These structures are probably the ones presenting a spectrum of AuNP dimers.

3.4.4 Overall assessment of the nanoparticle films produced

The different samples present roughly the same structures, indicating that this process works for various nanoparticle sizes. Nonetheless, when compared to the films produced reported by the literature[2], these results leave much to desire, since the film of nanoparticles is not homogeneous throughout the entire surface.

This could be due to the concentrations of nanoparticles used not being optimized. In order to achieve this, confined areas could be implemented in order to contain the droplet in a certain area, which would allow for the number of nanoparticles needed to cover that area. However, this should be done with caution, since it could lead to the stacking of nanoparticles in multilayer structures.

Nonetheless, this deposition method as proved capable of producing organised layers of AuNPs. The next step was to test the fluorescence enhancing capabilities of the films formed.

3.5 Fluorescence enhancement of BF1-BT in 2-D organized AuNP film

The enhancing capabilities of the nanoparticle films produced was conducted using BF1-BT as the test fluorophore. The surface selected was composed of 80nm particles.

A FLIM image taken of the surface is shown in figure 3.50.

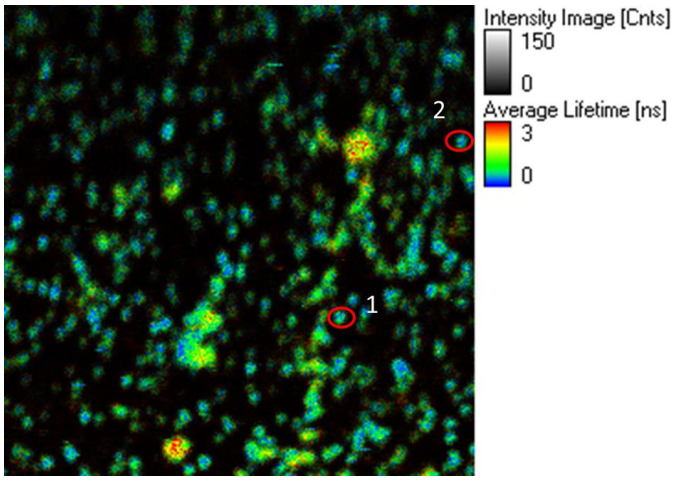

Figure 3.50- FLIM image of a glass slide with a film deposited of AuNPs sized 80nm immersed in PBS buffer. Image was recorded with dimensions of 80x80µm using laser excitation at 482nm (with a power of 50 kW/cm$^{2)}$.

Following this, emission spectrum for some points in the surface was taken. Below, in figure 3.51, are two examples of emission spectrum corresponding to points 1 and 2, as identified in figure 3.50.

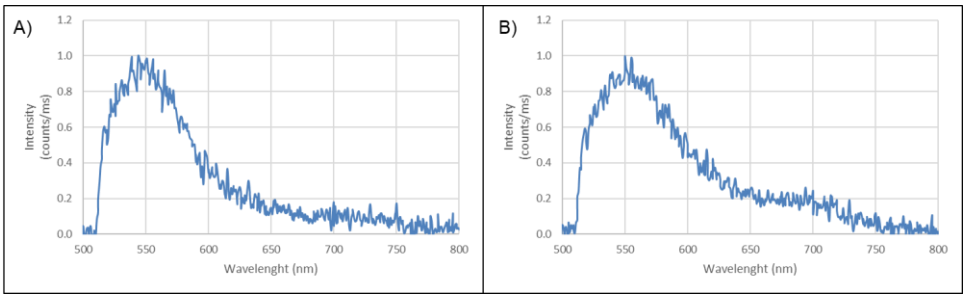

Figure 3.51 – Emission spectra for points 1 and 2 as identified in figure 3.50, A) and B) respectively.

As it is possible to see, the spectra obtained have some major differences. The spectrum in figure 3.51-B appears to indicate the presence of a dimerized structure in this point of the surface. The presence of the second peak/shoulder located at higher wavelengths suggests that two nanoparticles are located close enough so that their individual LSPs are able to interact and therefore present a spectrum similar to that of a dimer. As for the spectrum in figure 3.51-A, it indicates the presence of a single nanoparticle. The laser was then changed to excitation at 639 nm and intensity time traces were acquired from the previously studied surface points before adding the fluorophore. These measurements served as controls to guarantee that no fluorescence intensity bursts were obtained, which in this case did not succeed.

The BF1-BT hybrid was then added with a concentration of 10nM and left to incubate on the surface for 1 hour, so that the thiols of the oligonucleotide chain could interact and attach onto the deposited AuNPs. After that time, the solution containing BF1-BT was removed and the same area was washed with PBS, followed by new measurements of intensity time trace taken in the same points.

Upon analysing this data, it was possible to observe that even in the time traces obtained for the AuNPs without BF1-BT hybrid, there was already some intensified fluorescent signal. Note that this signal is attributed to the interaction of impurities present on the surface with the metallic nanostructures. This

was confirmed by FCS measurements with the focus positioned inside the PBS solution (10 µm above the surface), which showed no comparable fluorescence signals.

In figure 3.52, it is shown the intensity time traces measured on point 2 of the surface, corresponding to spectrum of figure 3.51-B, before and after the addition of BF1-BT.

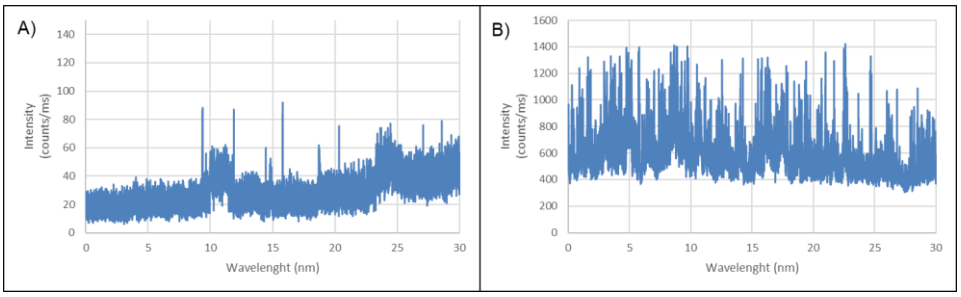

Figure 3.52 – Variation of the fluorescence intensity through time of point 2, prior (A) and after (B) the addition of BF1-BT.

The increase in the fluorescent signal that is observed between the measurements prior and after the addition of BF1-BT complex addition clearly shows enhanced emission due to interaction of BF1-BT with the plasmonic film. However, no quantitative conclusions can be drawn, due to the signal already present in the control situation, making it questionable the attribution of the emission to either the fluorophore of BF1-BT or the impurities on the surface that are responsible for the fluorescence burst in the control situation.

When analysing the data corresponding to single AuNPs, correspondent to in point 1 (see figure 3.53), it was noted that the intensities obtained for this point, are much higher than what is expected of a single AuNP. So, despite the emission spectrum appearing to be that of a single AuNP, in fact this nanoparticle must be in a film, where the AuNPs do not have an optimum spacing distance from each other for the interaction of their LSPs, resulting in a “fake” single AuNP spectrum. Nonetheless, a lower number of events of fluorescence and of lower intensity are observed in both the control and test measurements of point 1, when compared to those of point 2.

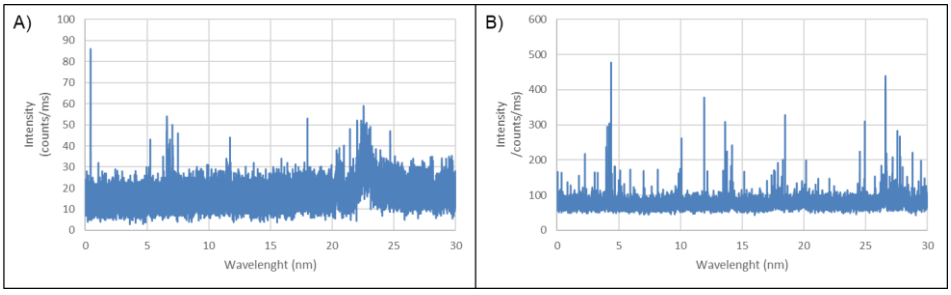

Figure 3.53 – Variation of the fluorescence intensity through time of point 1, prior (A) and after (B) the addition of BF1-BT.

This was expected since the fluorescence enhancing capabilities produced, of dimerized AuNPs or single AuNPs, due to the different intensities of the electric fields produced being quite different. Despite that, since the surface is contaminated it is impossible to distinguish if these fluorescence signals are being emitted by the contamination or the fluorophore. Therefore, the determination of enhancement factors is not reliable.

This contamination could have occurred at any point of the surface preparation. Despite all the measures taken to try removing as many contaminants possible, from the stringent glass surface washing procedures to the use of spectroscopic grade ethanol and toluene for the deposition. In the future, to try removing these contaminations, tests should be performed to guarantee that all of the reagents used are free of fluorescent signal. In order to do so, FCS measurements of those solvents could be performed. Also, an extra step of UV/Ozone exposure treatment could be implemented after the nanoparticle deposition on the surface. However, it is not known what the effect of this could have on the AuNPs attachment to the surface, which could eventually create a problem when performing the fluorescent enhancement assays, due to the risk that the AuNPs would be washed from the surface whenever there was a removal or addition of solutions to the glass slide.

However, since this experiment was performed on an advance stage of this project duration, there was not enough time to try and identify the contamination source and redo the experiment.

Nevertheless, it is clear that the intensity of the fluorescent signal increased significantly with the addition of the fluorophore, suggesting that it is interacting with the AuNPs on the surface and inducing a strong fluorescence enhancement effect.

3.6 Fluorescence enhancement of BF1-BD2-TD in 2-D organized AuNP film

As mentioned previously, the molecular beacon BF1-BD2 is composed by a DNA hairpin probe that in the closed conformation (i.e. absence of target TD) has the fluorophore (Atto-647N) positioned close to a quencher (QSY-21). Upon hybridization of the loop region of the DNA hairpin in BF1-BD2 with the target TD sequence, the hairpin opens and fluorescence is recovered. The molecular beacon functionality for sensing TD sequence was tested using the same surface as in the previous section (chapter 3.5).

In this experiment, the action of BF1-BD2 molecular beacon was assessed by taking multiple CFM images of the surface, before and after the addition of the molecular beacon, and after the target was introduced (figure 3.54). Below, images of the steps just described are shown. It is possible to observe an increase in intensity, due to the presence of BF1-BD2, which contains the fluorophore with quenched fluorescence, and then another increase due to opening of the DNA hairpin triggering the appearance of fluorescence after the target is added.

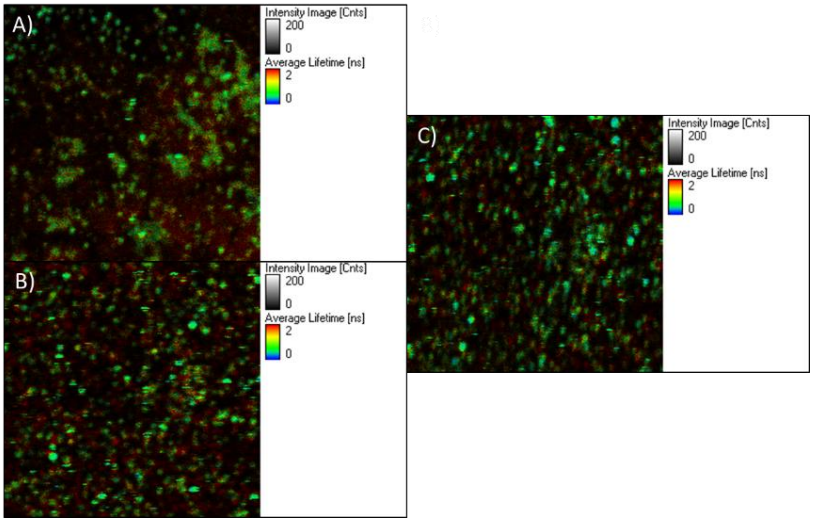

Figure 3.54 - FLIM image of a glass slide with deposited 80nm AuNPs. Image obtained in PBS with dimensions of 80x80µm, with the laser of 639nm with a 0.024µm/pixel resolution. Images related to before the addition of BF1-BD2 (A), after (B) and after the addition of the target (C).

The intensities of these images were then analysed using the intensity-lifetime histograms (present in figure 3.55). The peak intensities of these histograms were averaged over 5 replicas acquired for each step, in order to calculate an average intensity, except for the control for which a single image was taken.

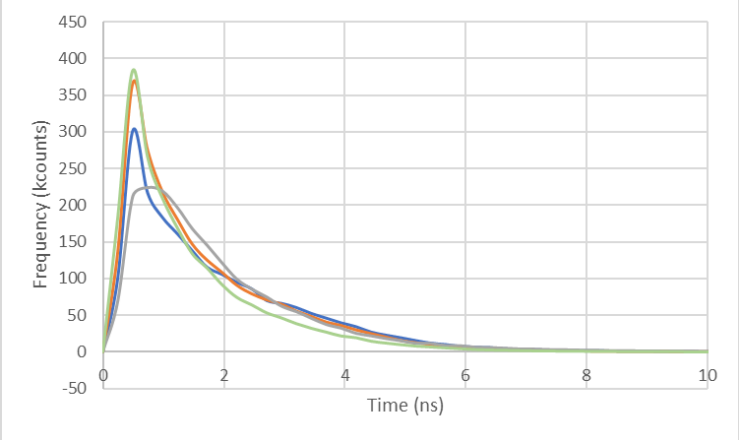

Figure 3.55 – Intensity-lifetime histogram of areas obtained before (grey) and after (blue) the addition of BF1-BD2, after the addition of the target (orange) and after 30 minutes of incubation (green).

In figure 3.55 the frequency of events with a specific lifetime is plotted, with this it is possible to assess the increase of the enhanced fluorescence since it will have a reduced lifetime when interacting with the nanoparticles, when compared to the free molecule. It is also possible to see, that in the control measurement, there are events with a higher lifetime, this is probably due to contamination present in the surface, as observed before.

The results obtained are present in table 3.9.

Table 3.9 – Average of the fluorescence intensities (with SD) obtained for each step of the experiment.

Measurements	Frequency (kcounts) (with SD)
Control	225
BF1-BD2 added	318 ± 12
TD added	340 ± 22
TD (After 30 minutes)	371 ± 15

In the control measurement, the intensity determined results from the emission of AuNPs and any impurities that might be present. When the molecular beacon BF1-BD2 was added, it was observed an increase in fluorescence due to its interaction with the nanoparticles present on the surface. The emission from BF1-BD2 is detectable because the fluorophore's emission is not completely quenched in the closed configuration.

After the addition of the target sequence TD, another increase in intensity was observed. This turn, the intensity increase was attributed to the beacon's conformational change from closed to open hairpin upon hybridization with the target.

After 30 minutes passed from the addition of TD, the area measurements were repeated and the analysis showed an increase in fluorescence intensity. This result suggests that more target molecules had time to hybridize, thus increasing the fluorescence signalling response.

These findings are in agreement with the fluorescence sensor design, as described in 1.4.2, and with data previously obtained by the research group hosting this project[55] (data present in annex 6.4).

This experiment demonstrated the potential of the plasmonic substrates developed here for the enhancement of fluorescence signalling in sensors for nucleic acid detection. However, in order to truly assess the influence of the metallic nanostructures on the fluorescence signals of the molecular beacon tested, it would be desirable to perform enhancement experiments as the ones previously reported in this document, i.e. experiments combining single-particle and single-molecule fluorescence detection.

4. Conclusions and future work

The fluorescence enhancing capabilities of metallic nanostructures, is a topic of interest for various research fields, as it could potentially lead to the enhanced detection of compounds that are weakly fluorescent or to enhance emission from fluorophore labels thus allowing to detect them at a much lower concentrations than it is possible nowadays[7]. For that reason, this project set out to produce nanoparticle films capable of serving as fluorescence enhancing substrates.

Throughout this work, the fluorescence enhancing properties of metallic nanostructures interacting with fluorophore molecules were assessed, producing results which are comparable to those predicted through theoretical simulations.

A method for producing closely packed organized AuNPs films was implemented with some degree of success. Even though, the film produced was not homogeneous, some areas presented the desired morphology. These films were then used to conduct fluorescence enhancement assays, either with only the fluorophore component of the molecular beacon or with the entire beacon structure. Despite, the contamination problems encountered in the first case, the results showed that large fluorescence signals were obtained from the fluorophore, but contaminations present precluded any further conclusions. The latter assay, using the entire beacon structure, also showed that it is possible to distinguish the presence of a target nucleic acid for the DNA hairpin probe used, by showing different fluorescent signal intensities when the target was either absent or present.

Despite this, there is still much room for improvement, either by optimizing the processes used or by applying different methods. For instance a promising method for nanoparticle deposition would make use of an electrospray to deposit a monolayer of gold nanoparticles in the air-liquid interface of in a Langmuir trough, and subsequently passing that monolayer onto a surface, thereby forming a Langmuir-Blodgett film[31]. However, this method could not be tested during the project due to time and material constraints.

The repetition of fluorescence enhancement assays using the nanoparticle films needs to be carried out, in order to properly assess the enhancement capabilities of such structures.

Another step to be taken in the future is the implementation of AuNPs films as plasmonic substrates into microchannels. This would allow testing the fluorescence enhancement effect under experimental conditions closer to the application envisioned for plasmonic substrates, which would be the demonstration of more sensitive lab-on-a-chip fluorescence-based sensors.

Below, in figure 3.56, are shown the steps corresponding to the implementation plan leading to the application of plasmonic nanostructures to build a microchip for DNA sensing with enhanced fluorescence signalling, and the contribution given by this thesis work.

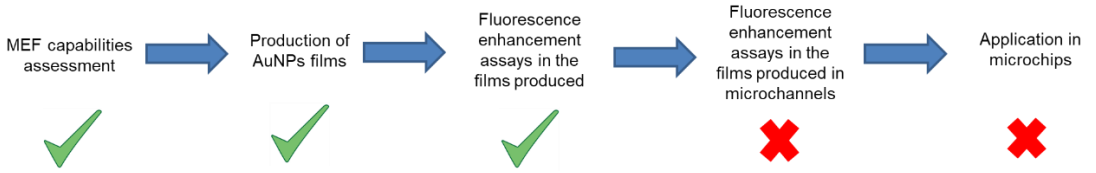

Figure 3.56 – Planification of the main steps to be taken to achieve the goal of applying the MEF capabilities of nanostructures to miniaturized microchip DNA sensing.

So, there is still a lot of work to be done before the implementation of this technology in miniaturized biosensors. However, the scientific community is working towards that goal, as shown by the significant research increase in this area throughout the years and the advancements made during that time.

5. References

[1] Lakowicz, Joseph R. "Radiative decay engineering: biophysical and biomedical applications." Analytical biochemistry 298.1 (2001): 1-24.

[2] Mitchell, Patrick S., et al. "Circulating microRNAs as stable blood-based markers for cancer detection." Proceedings of the National Academy of Sciences 105.30 (2008): 10513-10518.

[3] Renz, Malte. "Fluorescence microscopy—A historical and technical perspective." Cytometry Part A 83.9 (2013): 767-779.

[4] Valeur, Bernard, and Mário Nuno Berberan-Santos. Molecular fluorescence: principles and applications. John Wiley & Sons, 2012.

[5] Lakowicz, Joseph R. "JR, Principles of Fluorescence Spectroscopy." (2006): 353-382.

[6] Lichtman, Jeff W., and José-Angel Conchello. "Fluorescence microscopy." Nature methods 2.12 (2005): 910.

[7] Taylor, Adam B., and Peter Zijlstra. "Single-molecule plasmon sensing: current status and future prospects." ACS sensors 2.8 (2017): 1103-1122.

[8] Würth, Christian, et al. "Relative and absolute determination of fluorescence quantum yields of transparent samples." Nature protocols 8.8 (2013): 1535.

[9] Drexhage, K. H. "Influence of a dielectric interface on fluorescence decay time." Journal of luminescence 1 (1970): 693-701.

[10] P. M. R. Paulo, D. Botequim, A. Jóskowiak, S. Martins, D. M. F. Prazeres, P. Zijlstra, S. M. B. Costa, "'Plasmon-enhanced fluorescence using DNA- assembled gold nanoparticle dimers,'" no. Poster Commun. 14th IUVSTA Sch. Nano-Optics Braga, Portugal (2016).

[11] Darvill, Daniel, Anthony Centeno, and Fang Xie. "Plasmonic fluorescence enhancement by metal nanostructures: shaping the future of bionanotechnology." Physical Chemistry Chemical Physics 15.38 (2013): 15709-15726.

[12] Puchkova, Anastasiya, et al. "DNA origami nanoantennas with over 5000-fold fluorescence enhancement and single-molecule detection at 25 μM." Nano letters 15.12 (2015): 8354-8359.

[13] Lermusiaux, Laurent, et al. "Reversible switching of the interparticle distance in DNA-templated gold nanoparticle dimers." ACS nano 6.12 (2012): 10992-10998.

[14] O. S. Lee, T. R. Prytkova, and G. C. Schatz, "Using DNA to link gold nanoparticles, polymers, and molecules: A theoretical perspective," J. Phys. Chem. Lett., vol. 1, no. 12, pp. 1781–1788, 2010.

[15] Zhang, Xu, et al. "Toward fast and quantitative modification of large gold nanoparticles by thiolated DNA: Scaling of nanoscale forces, kinetics, and the need for thiol reduction." The Journal of Physical Chemistry C 117.30 (2013): 15677-15684.

[16] Idowu, Mopelola, Ji-Yao Chen, and Tebello Nyokong. "Photoinduced energy transfer between water-soluble CdTe quantum dots and aluminium tetrasulfonated phthalocyanine." New Journal of Chemistry 32.2 (2008): 290-296.

[17] Noreña-Franco, Luis E., and Frank Kvasnik. "Near-infrared optical detection of acids in atmospheric air by phthalocyanine dyes in polymer films." Analyst 121.8 (1996): 1115-1118.

[18] Macdonald, Ian J., and Thomas J. Dougherty. "Basic principles of photodynamic therapy." Journal of Porphyrins and Phthalocyanines 5.02 (2001): 105-129.

[19] Vietz, Carolin, et al. "Synergistic Combination of Unquenching and Plasmonic Fluorescence Enhancement in Fluorogenic Nucleic Acid Hybridization Probes." Nano letters 17.10 (2017): 6496-6500.

[20] Zhou, Zhenpeng, et al. "A distance-dependent metal-enhanced fluorescence sensing platform based on molecular beacon design." Biosensors and Bioelectronics 52 (2014): 367-373.

[21] Li, Hui, et al. "Silver nanoparticle-enhanced fluorescence resonance energy transfer sensor for human platelet-derived growth factor-BB detection." Analytical chemistry 85.9 (2013): 4492-4499.

[22] Cheng, Yunan, et al. "Fluorescence near gold nanoparticles for DNA sensing." Analytical chemistry 83.4 (2011): 1307-1314.

[23] Westphal, Volker, et al. "Video-rate far-field optical nanoscopy dissects synaptic vesicle movement." Science 320.5873 (2008): 246-249.

[24] Kolmakov, Kirill, et al. "Red-emitting rhodamine dyes for fluorescence microscopy and nanoscopy." Chemistry–A European Journal 16.1 (2010): 158-166.

[25] Isaacoff, Benjamin P., and Keith A. Brown. "Progress in Top-Down Control of Bottom-Up Assembly." (2017): 6508-6510.

[26] Choi, Wee Kiong, et al. "A combined top-down and bottom-up approach for precise placement of metal nanoparticles on silicon." Small 4.3 (2008): 330-333.

[27] A. R. Trindade Antunes, “Plasmonic enhancement of Gold Nanoparticles in a microfluidic biochip” (2016).

[28] Kim, Jin Young, et al. "Two-Dimensional Nanoparticle Supracrystals: A Model System for Two-Dimensional Melting." Nano letters 16.2 (2016): 1352-1358.

[29] Kim, Jin Young, Shilpa Raja, and Francesco Stellacci. "Evolution of Langmuir film of nanoparticles through successive compression cycles." Small 7.17 (2011): 2526-2532.

[30] Serrano-Montes, Ana B., et al. "A general method for solvent exchange of plasmonic nanoparticles and self-assembly into SERS-active monolayers." Langmuir 31.33 (2015): 9205-9213.

[31] Nie, Hua-Li, et al. "High-Yield Spreading of Water-Miscible Solvents on Water for Langmuir–Blodgett Assembly." Journal of the American Chemical Society 137.33 (2015): 10683-10688.

[32] Solís, Diego M., et al. "Optimization of nanoparticle-based SERS substrates through large-scale realistic simulations." ACS photonics 4.2 (2017): 329-337.

[33] Fu, Qiang, Guangjun Ran, and Weilin Xu. "Direct self-assembly of CTAB-capped Au nanotriangles." Nano Research 9.11 (2016): 3247-3256.

[34] Liebig, Ferenc, et al. "Deposition of gold nanotriangles in large scale close-packed monolayers for X-ray-based temperature calibration and sers monitoring of plasmon-driven catalytic reactions." ACS applied materials & interfaces 9.23 (2017): 20247-20253.

[35] Enderlein, Jörg, et al. "Performance of fluorescence correlation spectroscopy for measuring diffusion and concentration." ChemPhysChem 6.11 (2005): 2324-2336.

[36] Hess, Samuel T., et al. "Biological and chemical applications of fluorescence correlation spectroscopy: a review." Biochemistry 41.3 (2002): 697-705.

[37] Haustein, Elke, and Petra Schwille. "Fluorescence correlation spectroscopy: novel variations of an established technique." Annu. Rev. Biophys. Biomol. Struct. 36 (2007): 151-169.

[38] Hill, Haley D., et al. "The role radius of curvature plays in thiolated oligonucleotide loading on gold nanoparticles." ACS nano 3.2 (2009): 418-424.

[39] Jin, Ping, Zhao Dai, and Tianrui Chang. "The Role of Bis (p-Sulfonatophenyl) Phenylphosphine in Stabilizing Gold Nanoparticles." AASRI International Conference on Industrial Electronics and Applications. 2015.

[40] Rhodamine, B. "Absolute Diffusion Coefficients: Compilation of Reference Data for FCS Calibration."

[41] Buschmann, Volker, et al. "Quantitative FCS: determination of the confocal volume by FCS and bead scanning with the microtime 200." Application Note PicoQuant GmbH, Berlin (2009).

[42] Krichevsky, Oleg, and Grégoire Bonnet. "Fluorescence correlation spectroscopy: the technique and its applications." Reports on Progress in Physics 65.2 (2002): 251.

[43] Demers, Linette M., et al. "A fluorescence-based method for determining the surface coverage and hybridization efficiency of thiol-capped oligonucleotides bound to gold thin films and nanoparticles." Analytical chemistry 72.22 (2000): 5535-5541.

[44] Zhang, Taishi, et al. "Single-particle spectroscopic study on fluorescence enhancement by plasmon coupled gold nanorod dimers assembled on DNA origami." The journal of physical chemistry letters 6.11 (2015): 2043-2049.

[45] Caldarola, Martín, Biswajit Pradhan, and Michel Orrit. "Quantifying fluorescence enhancement for slowly diffusing single molecules in plasmonic near fields." The Journal of chemical physics 148.12 (2018): 123334.

[46] Punj, Deep, et al. "Self-assembled nanoparticle dimer antennas for plasmonic-enhanced single-molecule fluorescence detection at micromolar concentrations." ACS photonics 2.8 (2015): 1099-1107.

[47] Thacker, Vivek V., et al. "DNA origami based assembly of gold nanoparticle dimers for surface-enhanced Raman scattering." Nature communications 5 (2014): 3448.

[48] Paulo, Pedro MR, et al. "Enhanced Fluorescence of a Dye on DNA-Assembled Gold Nanodimers Discriminated by Lifetime Correlation Spectroscopy." The Journal of Physical Chemistry C 122.20 (2018): 10971-10980.

[49] Ortega, A., and J. Garcıa de la Torre. "Hydrodynamic properties of rodlike and disklike particles in dilute solution." The Journal of chemical physics 119.18 (2003): 9914-9919.

[50] Dulkeith, E., et al. "Gold nanoparticles quench fluorescence by phase induced radiative rate suppression." Nano letters 5.4 (2005): 585-589.

[51] Schneider, Grégory, et al. "Distance-dependent fluorescence quenching on gold nanoparticles ensheathed with layer-by-layer assembled polyelectrolytes." Nano letters 6.3 (2006): 530-536.

[52] Dulkeith, E., et al. "Fluorescence quenching of dye molecules near gold nanoparticles: radiative and nonradiative effects." Physical review letters 89.20 (2002): 203002.

[53] Anger, Pascal, Palash Bharadwaj, and Lukas Novotny. "Enhancement and quenching of single-molecule fluorescence." Physical review letters 96.11 (2006): 113002.

[54] Khatua, Saumyakanti, et al. "Resonant plasmonic enhancement of single-molecule fluorescence by individual gold nanorods." ACS nano 8.5 (2014): 4440-4449.

[55] Pedro M. R. Paulo, David Botequim, Rui Oliveira-Silva, Duarte M. F. Prazeres, Alexandra P. Francisco, César A. T. Laia, João P. Conde, and Sílvia M. B. Costa, "Anisotropic Gold Nanoantennas for Enhancing Fluorescence Detection: from Single to Dimer Nanoparticles", oral communication at 6th Jornadas Ibéricas de Fotoquímica, Aveiro, Portugal (2018).

[56] Zijlstra, Peter, Pedro MR Paulo, and Michel Orrit. "Optical detection of single non-absorbing molecules using the surface plasmon resonance of a gold nanorod." Nature nanotechnology 7.6 (2012): 379.

[57] Munechika, Keiko, et al. "Spectral control of plasmonic emission enhancement from quantum dots near single silver nanoprisms." Nano letters 10.7 (2010): 2598-2603.

[58] Chen, Yeechi, Keiko Munechika, and David S. Ginger. "Dependence of fluorescence intensity on the spectral overlap between fluorophores and plasmon resonant single silver nanoparticles." Nano letters 7.3 (2007): 690-696.

[59] Teixeira, Raquel, et al. "Plasmon-enhanced emission of a phthalocyanine in polyelectrolyte films induced by gold nanoparticles." The Journal of Physical Chemistry C 115.50 (2011): 24674-24680.

[60] Laia, Cesar AT, et al. "Electron-transfer kinetics in sulfonated aluminum phthalocyanines/cytochrome c complexes." The Journal of Physical Chemistry B 108.22 (2004): 7506-7514.

[61] D. Botequim, P. M. R. Paulo, D. M. F. Prazeres, and S. M. B. Costa, “Gold Nanorods Conjugated with Fluorescently-Labeled DNA’s: Highly Loaded Dye-Nanoparticles,” in Gordon Research Conference, From Fundamentals to Applications of Collective Excitations in Nanostructured Materials- Massachusetts, EUA (2018).

6. Annex

6.1 AuNPs characterization

Table 6.10 – AuNPs 20nm diameter characterization according to the supplier specification sheet.

A11-20-CIT (Accurate Spherical Gold Nanoparticles) – Nanopartz	
Capping agent	Citrate
Solution (nm)	H2O Milli-Q (18,2 MΩ·cm)
Diameter (TEM, DLS)	20
Optical density	1
Concentration (nanoparticles/mL)	6,82E11
Molar Extinction Coefficient ($M^{-1}cm^{-1}$)	8,8E8
SPR peak (nm)	519 nm

Table 6.11 – AuNPs 40nm diameter characterization according to the supplier specification sheet.

A11-40-CIT (Accurate Spherical Gold Nanoparticles) – Nanopartz	
Capping agent	Citrate
Solution (nm)	H2O Milli-Q (18,2 MΩ·cm)
Diameter (TEM, DLS)	40
Optical density	1
Concentration (nanoparticles/mL)	8,69E10
Molar Extinction Coefficient ($M^{-1}cm^{-1}$)	6,9E9
SPR peak (nm)	527 nm

Table 6.12 – AuNPs 80nm diameter characterization according to the supplier specification sheet.

A11-80-CIT (Accurate Spherical Gold Nanoparticles) – Nanopartz	
Capping agent	Citrate
Solution (nm)	H2O Milli-Q (18,2 MΩ·cm)
Diameter (TEM, DLS)	80
Optical density	1,2
Concentration (nanoparticles/mL)	1,33E10
Molar Extinction Coefficient ($M^{-1}cm^{-1}$)	5,41E10
SPR peak (nm)	550 nm

6.2 DNA strands characterization

Table 6.13 – PA15 DNA strand characterization according to the supplier specification sheet.

PA 15: 5' – aaa aaa aaa agt cca gac tcc tac – 3'	
Length (nt)	25
Melting Temperature (ºC)	54
GC content (%)	36
Molar Extinction Coefficient ($M^{-1}cm^{-1}$)	3,08E5
Molecular weight (g/mol)	7846
Purification	HPLC
5' Modifications	Thiol C6
3' Modifications	-

Table 6.14 – SA15 DNA strand characterization according to the supplier specification sheet.

SA 15: 5' – aaa aaa aaa acg tag gag tct gga – 3'	
Length (nt)	25
Melting Temperature (ºC)	54
GC content (%)	36
Molar Extinction Coefficient ($M^{-1}cm^{-1}$)	3,2E5
Molecular weight (g/mol)	7963
Purification	HPLC
5' Modifications	Thiol C6
3' Modifications	-

Table 6.15 – PAF30 DNA strand characterization according to the supplier specification sheet.

PAF30: 5' – aaa aaa aaa aaa agt taa tac ctt tgc tca ttg acg tta – 3'	
Length (nt)	40
Melting Temperature (ºC)	65
GC content (%)	25
Molar Extinction Coefficient ($M^{-1}cm^{-1}$)	4,9E5
Molecular weight (g/mol)	13052
Purification	HPLC
5' Modifications	Thiol C6
3' Modifications	6-Fam

Table 6.16 – SAF30 DNA strand characterization according to the supplier specification sheet.

SAF30: 5' – aaa aaa aaa agt aac gtc aat gag caa agg tat taa– 3'	
Length (nt)	40
Melting Temperature (ºC)	65
GC content (%)	25
Molar Extinction Coefficient ($M^{-1}cm^{-1}$)	5,1E5
Molecular weight (g/mol)	13151
Purification	HPLC
5' Modifications	Thiol C6
3' Modifications	6-Fam

Table 6.17 – BF1 DNA strand characterization according to the supplier specification sheet.

BF1: 5' – gag tct gga c– 3'	
Length (nt)	10
Melting Temperature (ºC)	32
GC content (%)	60
Molar Extinction Coefficient ($M^{-1}cm^{-1}$)	1,1E5
Molecular weight (g/mol)	4060
Purification	HPLC
5' Modifications	ATTO-647N
3' Modifications	Thiol C6

Table 6.18 – BT DNA strand characterization according to the supplier specification sheet.

BT: 5' – gtc cag act c– 3'	
Length (nt)	10
Melting Temperature (°C)	32
GC content (%)	60
Molar Extinction Coefficient ($M^{-1}cm^{-1}$)	1E5
Molecular weight (g/mol)	3181
Purification	HPLC
5' Modifications	Thiol C6
3' Modifications	-

Table 6.19 – TD RNA strand characterization according to the supplier specification sheet.

TD: 5' – cuc ucc gag aac agg ccu cga cuu caa– 3'	
Length (nt)	27
Melting Temperature (°C)	65
GC content (%)	55
Molar Extinction Coefficient ($M^{-1}cm^{-1}$)	2,9E5
Molecular weight (g/mol)	8547
Purification	HPLC
5' Modifications	-
3' Modifications	-

6.3 Buffers used for dimerization protocol

Table 6.20 – TBE 5x

Reagents	**Quantity**
Trizma-Base	0,446 M
Boric Acid	0,445M
EDTA	10mM
pH = 8, adjusted with Sodium Hydroxide	

Table 6.21 – NaCl-Citrate Buffer.

Reagents	**Quantity**
Sodium Citrate Tribasic Dihydrate	100 mM
Sodium Chloride	700 mM
pH = 3, adjusted with hydrochloric acid	

6.3 PAF30 and SAF30 calibration curves

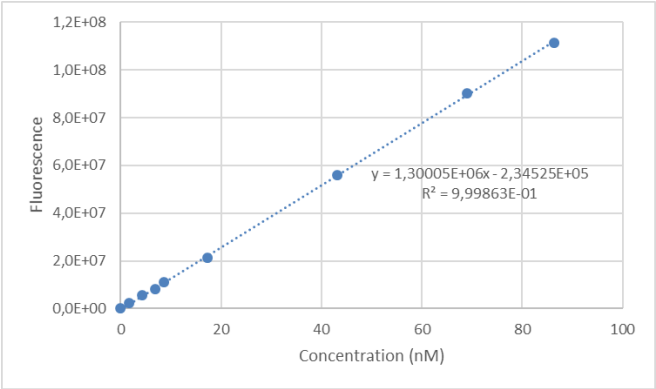

Figure 6.57 – Calibration curve correlating fluorescence with concentration for PAF30 using an excitation of 470nm and a 2nm slit.

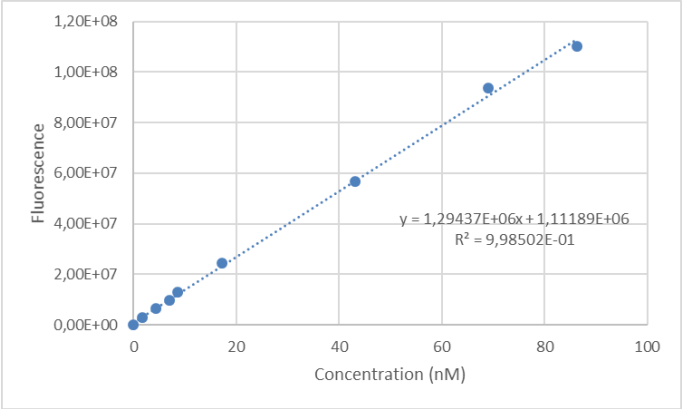

Figure 6.58 – Calibration curve correlating fluorescence with concentration for SAF30 using an excitation of 470nm and a 2nm slit.

6.4 BF1-BD2-TD actuation mechanism assay

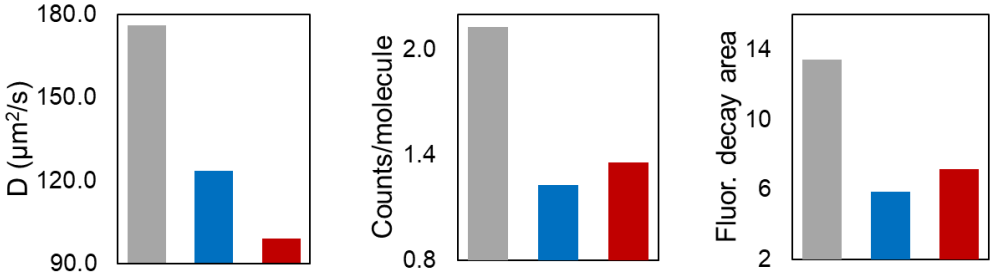

Figure 6.59 – Calibration curve correlating fluorescence with concentration for SAF30 using an excitation of 470nm and a 2nm slit.